



<https://theses.gla.ac.uk/>

Theses Digitisation:

<https://www.gla.ac.uk/myglasgow/research/enlighten/theses/digitisation/>

This is a digitised version of the original print thesis.

Copyright and moral rights for this work are retained by the author

A copy can be downloaded for personal non-commercial research or study,  
without prior permission or charge

This work cannot be reproduced or quoted extensively from without first  
obtaining permission in writing from the author

The content must not be changed in any way or sold commercially in any  
format or medium without the formal permission of the author

When referring to this work, full bibliographic details including the author,  
title, awarding institution and date of the thesis must be given

Enlighten: Theses

<https://theses.gla.ac.uk/>  
[research-enlighten@glasgow.ac.uk](mailto:research-enlighten@glasgow.ac.uk)

ELASTIC PHOTOPRODUCTION OF NEUTRAL PIONS FROM HELIUM.

BY

P. PALIT

DEPARTMENT OF NATURAL PHILOSOPHY,

UNIVERSITY OF GLASGOW.

PRESENTED TO THE UNIVERSITY OF GLASGOW IN MAY 1958 AS

A THESIS FOR THE DEGREE OF DOCTOR OF PHILOSOPHY.

ProQuest Number: 10656366

All rights reserved

INFORMATION TO ALL USERS

The quality of this reproduction is dependent upon the quality of the copy submitted.

In the unlikely event that the author did not send a complete manuscript and there are missing pages, these will be noted. Also, if material had to be removed, a note will indicate the deletion.



ProQuest 10656366

Published by ProQuest LLC (2017). Copyright of the Dissertation is held by the Author.

All rights reserved.

This work is protected against unauthorized copying under Title 17, United States Code  
Microform Edition © ProQuest LLC.

ProQuest LLC.  
789 East Eisenhower Parkway  
P.O. Box 1346  
Ann Arbor, MI 48106 – 1346

## PREFACE.

The following describes research work done by the author during the period October 1955 to May 1958, in the Department of Natural Philosophy, University of Glasgow, towards a Ph.D. degree. He was assisted in his first year by Mr. R.W.P. McWhirter, with whom the apparatus (the target and the detector) was jointly developed. The author, however, was individually responsible for building most of the electronics, as also for the actual collection, and analysis of the entire experimental data. He would, of course, like to express his deep gratitude to his supervisor Dr. E.H. Bellamy for his constant help and guidance throughout the whole course of the experiment. He would also like to thank Dr. K.D.C. Stoodley for communicating the results of his theoretical calculations prior to publication, and for many helpful discussions in connection with their clarification.

The use of the apparatus has been extended to measure the yields of  $\text{He}^3$  and  $\text{He}^4$  particles from the high energy photodisintegration of Oxygen, Argon and Krypton by Mr. I.M.H. Preston. The appendix gives the results of the experiment with Oxygen, in which the author had also taken part.

In conclusion, the author would like to thank Professor P.I. Dee, F.R.S., for his keen interest in the work, the synchrotron crew<sup>d</sup> under Dr. McFarlane for running the synchrotron for him, and the various laboratory and workshop technicians under Mr. J.T. Lloyd, R. Irvine, T. Pollock and W. Simpson for help in building the apparatus, and in maintaining and servicing electronic equipment. He is also grateful to the University of Glasgow for partial financial assistance during the third year of his research.

## CONTENTS.

	<u>Page</u>
<u>CHAPTER I</u> - INTRODUCTORY REVIEW OF PHOTOMESON PRODUCTION.	
Section A - Photoproduction from a Single Nucleon.	I
Section B - Photoproduction from Deuteron.	10
Section C - Elastic Photoproduction of Neutral Pions from Helium.	16
<u>CHAPTER II</u> - DESCRIPTION OF THE APPARATUS.	
Section A - The Target.	26
Section B - The Detecting System.	
(i) Initial Stages	30
(ii) Final Form.	33
Section C - The Electronic Arrangement for Recording the Information.	45
<u>CHAPTER III</u> - ANALYSIS OF THE DATA AND EVALUATION OF CROSS-SECTIONS.	
Section A - General Procedure.	54
Section B - Experimental Confirmation with Polonium $\alpha$ -Particles	57
Section C - Experimental Confirmation in a Run on the Synchrotron.	60
Section D - Calculation of Cross-section.	63

<u>CHAPTER IV</u>	-	RESULTS.	
Section A	-	Photomeson Production Experiment.	
		(i) $\theta = 20^\circ$	70
		(ii) $\theta = 30^\circ$	74
		(iii) $\theta = 40^\circ$	75
		(iv) $\theta = 50^\circ$ .	77
Section B	-	The He <sup>3</sup> Cross-sections.	79
<u>CHAPTER V</u>	-	INTERPRETATION AND DISCUSSION.	80
CONCLUSION	-		92
APPENDIX	-	He <sup>3</sup> and He <sup>4</sup> Yields from the Photodisintegration of Oxygen <sup>16</sup> .	94
REFERENCES			

## Section (A) Photoproduction from a Single Nucleon.

Production of  $\pi$  mesons in nuclear collisions of high energy gamma-rays has been studied extensively with the bremsstrahlung beams from betatrons and synchrotrons, and in fact led to the first conclusive evidence for the existence of the  $\pi^0$  meson. <sup>1,2)</sup> For, next to scattering, photoproduction is the most important method of studying the meson-nucleon interaction, although the interpretation of the results is not quite so simple. While the former involves only the phase shifts at a particular energy, the photoeffect also involves the interaction of the electromagnetic field with the nucleon and meson, as well as the wavefunction of the nucleon ground state. The two phenomena are, however, inter-related, and the predominance of one partial wave in scattering is also expected to show up in the photoproduction cross-sections.

Both  $\pi^+$  and  $\pi^0$  mesons have been observed from the photonic bombardment of hydrogen, i.e. both the reactions



have been studied. Being two-body processes, the measurement of the angle and energy of one of the recoiling particles uniquely specifies the kinematics of either reaction including the energy of the initiating  $\gamma$ -ray, which is otherwise not known because of the continuous nature of the

bremsstrahlung spectrum. In case of charged meson production, the recoiling particle chosen is invariably the  $\pi^+$ . The first experiments in this line were done by Steinberger et. al. <sup>3-5)</sup> The measurements have since been repeated and improved upon, by many workers. The most complete investigations are those done at Cal. Tech. <sup>6,7)</sup> and Cornell. <sup>8)</sup> Two different methods have been used to determine the meson energy at a given angle, viz (i) magnetic deflection to define the momentum, and (ii) a counter telescope to define the range, of the meson.

For studying the production of neutral mesons from hydrogen (which will be discussed in somewhat greater detail), several methods are available, viz -

- (1) Simultaneous detection of the two  $\gamma$ -rays from the decay of the  $\pi^0$ ; <sup>2)</sup>
- (2) Observation of the recoil proton in coincidence with a decay  $\gamma$ ; <sup>9-11)</sup>
- (3) Observation of the proton alone; <sup>12-16)</sup>
- (4) Observation of only 1  $\gamma$ -ray; <sup>17-19)</sup>

Though all the different methods have been used by different workers (3) is by far the simplest and the most straightforward, and has been used for the most complete and accurate measurements. These include work of three different groups, Goldschmidt - Clermont et. al. <sup>13)</sup> of M.I.T., and Corson et. al. <sup>16)</sup> and Oakley, Walker <sup>14)</sup> of Cal. Tech. The first two used a

target of hydrogen gas at a high pressure of several hundred pounds/sqaure inch and low temperature ( $-60^{\circ}\text{C}$ ), and used nuclear emulsions to detect the recoil protons. A background varying between 5% and 30% had to be substracted. These were mostly photoprotons arising out of the Oxygen and Nitrogen impurities in the gas. Their contribution was estimated from the yields and angular distributions as measured by other workers, together with the observed background at angles greater than what was dynamically permissible for the  $\pi^0$  production process. The nuclear Compton effect, i.e., the process  $\gamma + p \rightarrow \gamma + p$  was assumed to be negligible.

Oakley and Walker identified the recoil proton at a laboratory angle by its momentum, as defined by magnetic deflection, and by its ionization loss in a scintillator. The latter served to distinguish between protons and pions. The target was hydrogen compressed to 2000 lbs/sq.inch at liquid nitrogen temperature. There was considerable background of protons without any hydrogen in the target. This had to be subtracted. All protons in the hydrogen-background difference were assumed to come from the production process.

Koester and Mills <sup>19)</sup> of Illinois have measured the total cross-section from threshold upwards, by detecting a single  $\gamma$ -ray from the decay of the  $\pi^0$ . Counting rates from a liquid hydrogen target at an angle of  $85^{\circ}$  to the  $\gamma$ -ray beam, were measured as the betatron peak energy was raised in

10 MeV steps, from 120 to 250 MeV. The photon difference method yielded the counting rate/incident photon as a function of photon energy. This counting rate/photon  $I_{850}$  was related to the photomeson production cross-section by integrating the spectrum of the decay photons over the detector efficiency, which was both calculated, as well as measured.

In its own rest-frame, the  $\pi^0$  decays isotropically into two photons, each of energy  $\frac{1}{2} \mu c^2$ . The Lorentz transformation from this frame to the photoproduction centre-of-mass system results in a unique relation between the energy of the photon, and the angle between the meson and photon directions. For  $\gamma$ 's emitted in a certain direction in the centre-of-mass system, an integration over all  $\pi^0$  directions is equivalent to an integration over the  $\gamma$ -ray energy spectrum; for the  $\pi^0$  energy is independent of angle in this system.

This  $\gamma$ -ray energy spectrum would, of course, depend on the angular distribution of the  $\pi^0$ 's. If the photomeson differential cross-section in centre-of-mass is assumed to be of the form

$$\sigma(\theta) = A + B \cos \theta + C \cos^2 \theta \quad (3)$$

then the total cross-section is given by

$$\sigma(\text{total}) = 4\pi \left( A + \frac{1}{3} C \right) \quad (4)$$

It was shown that in the resulting expression for  $I_{850}$ , the

term involving B was negligibly small, while the ratio of the coefficient of C to that of A was approximately  $1/3$ . Thus the data were essentially a measure of  $\sigma$  total. Since the ratio was not exactly  $1/3$  at all energies, a value had to be assumed for  $C/A$ , i.e. for the shape of the angular distribution. But the results were claimed to be insensitive to this value. Thus changing this ratio from  $-0.6$  to  $-1.0$  altered  $\sigma$  total by only 10% at 240 MeV, and by successively smaller percentages at the lower energies. These authors also measured the absolute differential cross-section at  $135^\circ$ , and combined it with the total cross-section data to obtain values of A, B and C.

Goldschmidt-Clermont's results consisted of angular distribution for meson centre-of-mass angles varying between  $45^\circ$  and  $160^\circ$ , for energy bands centred at 220, 260 and 305 MeV; and also total cross-sections between 175 and 325 MeV, obtained by extrapolating the measured angular distribution, assuming no higher power of  $\cos \theta$  than the second.

Oakley, Walker and Corson et. al's. experiments which were both done at Cal. Tech., using the same machine, and the same beam calibration, covered the photon energy range 240-480 MeV, but were mutually supplementary. The formers' data were restricted to pion centre-of-mass angles greater than  $70^\circ$  ( $70^\circ$ - $153^\circ$ ) owing to the higher value for the minimum detectable proton energy. Self-absorption in the target and counters set this low energy limit at about 25 MeV.

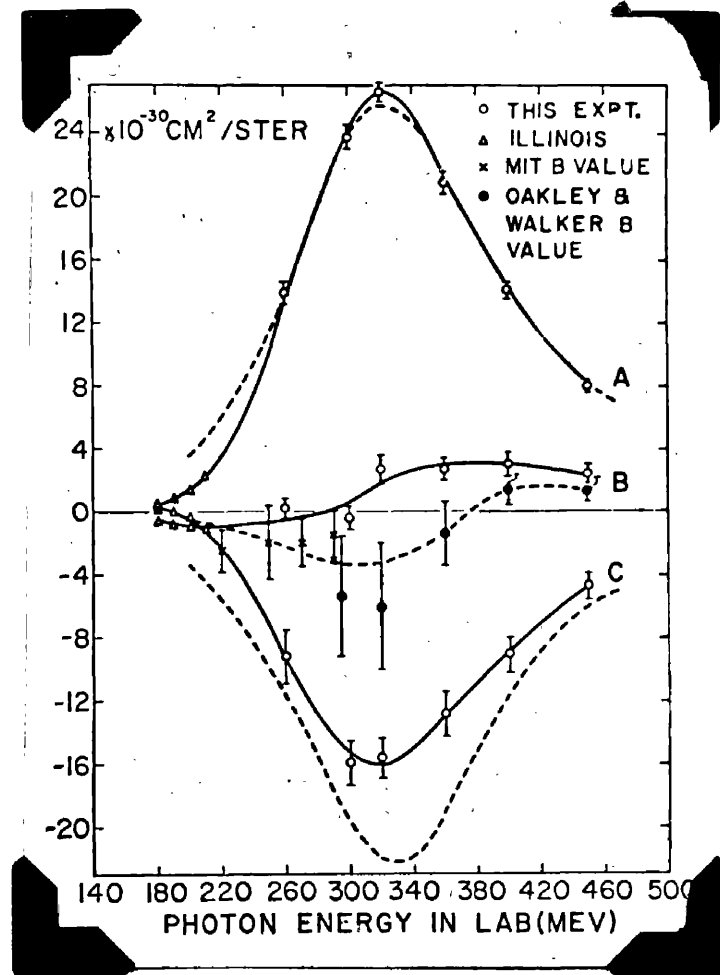


Fig. I. Coefficients of the c.m. angular distribution  $\frac{d\sigma}{d\Omega_{c.m.}} = A + B \cos^2 \theta + C \cos^4 \theta$  for the reaction  $\gamma + P \rightarrow \pi^0 + P$  plotted as a function of photon energy. "This experiment" refers to the combined data of Oakley Walker & Corson et. al. The solid curves are visual fits to these & the Illinois measurements at low energies. (The dashed curves are to be ignored.)

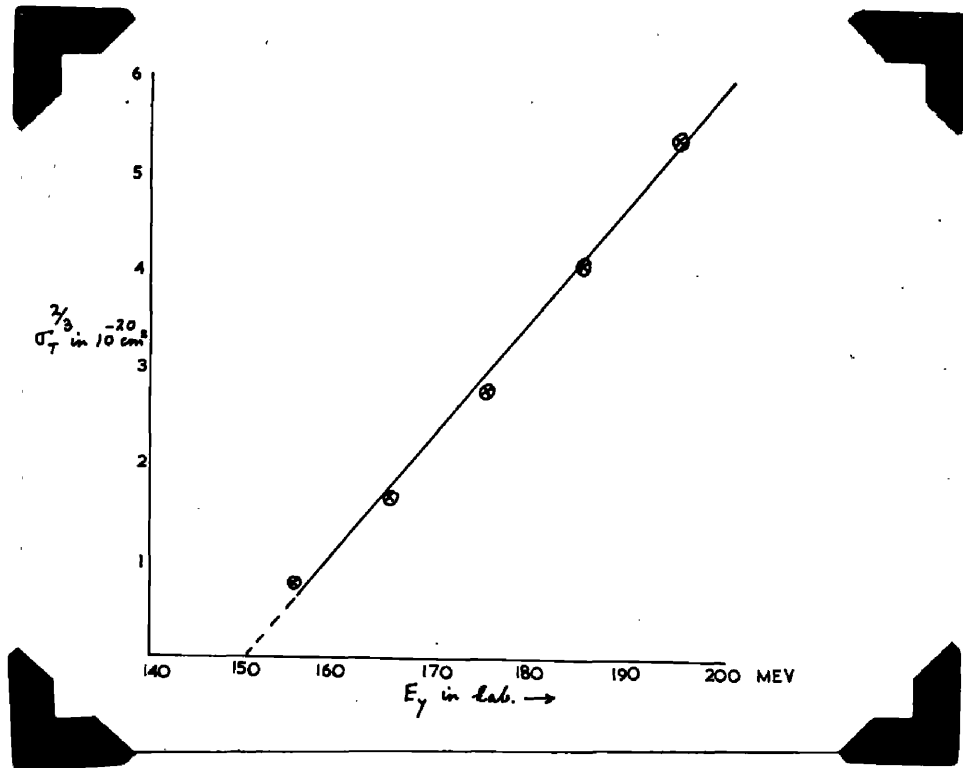


Fig.II. A plot of the Illinois measurements of the total cross\_section for photoproduction of  $\pi^0$  from hydrogen. The crosses are obtained from a smooth excitation function drawn through the experimental points.

Corson et.al. who placed emulsions right within the target gas could go down to a minimum recoil energy of 5 MeV. This enabled them to measure the differential cross-section for pion angles as low as  $26^\circ$  in centre-of-mass. In the region where the two experiments overlap ( $\theta = 90^\circ$ ) there is good mutual agreement in their results.

The combined data have been analysed in the form given by eqn. (3). Fig. I shows the results together with some relevant data from other workers. The coefficients A, B and C, have been plotted as functions of the photon energy in the laboratory system,  $E_\gamma$ . Also in Fig. II is a plot of  $\sigma^{\frac{2}{3}}$  total against  $E_\gamma$ , based on the Illinois measurements of total cross-section. Near threshold, this is observed to be a straight line which extrapolates very nearly to zero at the correct threshold of  $\sim 145$  MeV. A plot of the M.I.T. total cross-sections also shows similar behaviour.

Thus the following general features in the results can be noted:-

(i) The total cross-section shows a fairly sharp maximum round about 320 MeV, which corresponds to the same centre-of-mass energy of the pion-nucleon system as the resonance in  $\pi^+p$  scattering viz.  $\sim 190$  MeV, which is due to an intermediate state of total angular momentum  $J = 3/2$  and total isotopic spin  $T = 3/2$ ;

(ii) In the expression for the angular distribution  $C/A = -3/5$  over a wide range of photon energies, and B is very small, but finite.

(iii) The cross-section near threshold varies very nearly as the cube of the meson-momentum, i.e. as  $(E_\gamma - E_0)^{3/2}$  where  $E_0$  is the threshold energy.

As shown by Bueckner and Watson <sup>20)</sup> and by Feld <sup>21)</sup>, the angular distribution of the emitted mesons is determined by both the multipole character of the absorbed radiation, and the total angular momentum. On the other hand, the energy variation of the cross-section near threshold depends only on the orbital angular momentum of the emitted meson.

Table I. Feld's chart on the Angular and Energy Distribution in the Photoproduction of  $\pi$  Mesons at Nucleons.

$\gamma$ -ray absorbed	Intermediate State		$l$ of $\pi$ -meson	$\frac{d\sigma(\theta)}{d\Omega}$	$\pi$ -momentum dependence near threshold
	J	Parity			
Magnetic Dipole	$1/2$	+	1	Constant	$P^3$
Magnetic Dipole	$3/2$	+	1	$2+3 \sin^2\theta$	$P^3$
Electric Dipole	$1/2$	-	0	Constant	P
Electric Dipole	$3/2$	-	2	$2+3 \sin^2\theta$	$P^5$
Electric Quadrupole	$3/2$	+	1	$1 + \cos^2\theta$	$P^3$
Electric Quadrupole	$5/2$	+	3	$1+6 \cos^2\theta - 5 \cos^4\theta$	$P^7$

Thus it varies linearly with meson momentum  $P$  for production into  $s$  states, and as third power for  $p$  states. The observed excitation function for  $\pi^0$ 's near threshold shows that there can be little  $s$  state production, and is compatible with almost pure  $p$  state. This leaves three possibilities; magnetic dipole absorption with  $J = 3/2$ ,  $J = 1/2$ , and electric quadrupole absorption with  $J = 3/2$ . If only one of these contributes, the observed angular distribution  $2+3 \sin^2\theta$ , requires that it be magnetic dipole absorption with  $J = 3/2$ . This is in contrast with charged pion production, where  $\sigma \propto (E_\gamma - E_0)^{1/2}$  near threshold, and the angular distribution is nearly isotropic in that region; which leads to the inference that there is a considerable admixture of both  $s$  and  $p$  states. It is to be noted that Feld's treatment is based on purely phenomenological considerations involving angular momentum and parity conservation requirement, and does not depend on any specific type of meson theory.

The role of isotopic spin is rather uncertain. Both  $T = 3/2$  and  $T = 1/2$  substates in  $J = 3/2$  will give rise to the observed angular distribution. However, from results of scattering experiments, the  $T = 3/2$  state is known to be of strong interaction, and the marked resonance in the total  $\pi^0$  cross-section at 320 MeV (where the cross-section drops off much more rapidly than  $\lambda^2$ ,  $\lambda$  being the wavelength of the incident photon) suggests strongly that at least in this

energy region, it is the  $T = 3/2$  substate which is predominant. The resonance is much less pronounced for  $\pi^+$  production as is to be expected, because of the diluting effect of the S-state.

Thus the overall conclusion would seem to be, that photoproduction of  $\pi^0$  from a free proton proceeds predominantly via magnetic dipole absorption of the incident  $\gamma$ -ray, leading to a resonant state of the pion nucleon system of angular momentum  $3/2$  and isotopic spin  $3/2$ ; though the non-zero value of B suggests that there is some interference with s-wave production.

## Section (B) Photoproduction from Deuteron.

Next to a free proton photoproduction from a free neutron should be theoretically, the most interesting and fundamental reaction to study. Since the deuteron is the nearest practical approach to a free neutron, both charged and neutral photopion production from deuteron have been extensively investigated. Thus comparable production of positive and negative mesons (Sands <sup>22</sup>) et. al.) from deuterium as well as a ratio varying between 1.7 to 2 for  $\frac{\sigma(\gamma\pi^0)_D}{\sigma(\gamma\pi^0)_H}$  (Cocconi et.al. <sup>23</sup>), Bingham <sup>24</sup>) et.al) suggest, at least qualitatively, that the neutron is as effective as the proton in both charged, and neutral meson production.

Of particular interest is the elastic photoproduction of  $\pi^0$ 's from deuteron, i.e. the process



in which the deuteron nucleus recoils intact. Being a two-body process, it is amenable to easy and exact experimental investigation. Chew and Lewis <sup>25</sup>) have developed a purely phenomenological theory for this process, based on the "impulse approximation". The fundamental assumptions are the following:-

(i) The incident photon shares its momentum with only one nucleon inside the nucleus.

(ii) The production amplitudes from the two nucleons are linearly superimposable and each is same as that from the corresponding free nucleon.

On this basis, these authors show, that

$$\left(\frac{d\sigma}{d\Omega}\right)_{D,e} = \left\{ \frac{2}{3} |\vec{k}_N + \vec{k}_P|^2 + |L_N + L_P|^2 \right\} |F(p)|^2 \quad (6)$$

$$\text{where } F(p) = \int \chi^2(r) e^{i\vec{p}\cdot\vec{r}/2} d\tau \quad (7)$$

is the form factor of the deuteron,  $\chi(r)$  its ground state wave function, and  $\vec{p}$  is the recoil momentum.  $\vec{k}$  is the matrix element for  $\pi^0$  production with spinflip of the nucleon. L that without spinflip. The subscripts N and P refer to production by neutrons and protons respectively.

The cross-section for production by a free proton, in the same rotation is

$$\left(\frac{d\sigma}{d\Omega}\right)_H = |\vec{k}_P|^2 + |L_P|^2 \quad (8)$$

The main interest in this experiment is a study of interference of proton and neutron production i.e. of the relative signs of the production amplitudes  $L_N$  and  $L_P$ , or  $\vec{k}_N$  and  $\vec{k}_P$ . The experimentally observed ratio of total cross-sections (23,24) from deuterium and hydrogen suggests that  $L_N = L_P$  and, or  $|\vec{k}_N| = |\vec{k}_P|$  according to which matrix element gives the main contribution. An independent measurement of the differential cross-section should serve as a check on this assumption, as well as on the validity of the so called impulse approximation, as applied to this problem.

Because of this theoretical interest, the experiment has been performed by several groups of workers. (26 - 29)

All of them used thin targets of deuterated paraffin, and essentially measured the angle and energy of the recoiling deuteron. A  $CD_2 - CH_2$  subtraction was used to eliminate the contribution of deuterons from the carbon in the target. In order to reduce this background contribution, so as to improve upon the statistics of subtraction, Wolfe et.al. <sup>26)</sup> of Cornell, and Baron <sup>27)</sup> et.al of M.I.T., whose experimental set-ups were almost identical, also detected one of the decay  $\gamma$ 's from the  $\pi^0$  in coincidence with the deuteron. For, the angular correlation between the two, which is definite in the case for hydrogen is largely absent from a structure like the carbon nucleus. This, however, had the disadvantage of reducing the counting rate, as well as of introducing an uncertainty in the evaluation of the absolute cross-section, because of the unknown efficiency of the  $\gamma$ -detector. The latter comprised of two factors; firstly the geometric efficiency for intercepting one of the decay photons from the  $\pi^0$ , which was maximum when the  $\gamma$ -telescope was placed in the direction of the recoiling  $\pi^0$  and which could be calculated fairly accurately from kinematical considerations; and secondly the intrinsic efficiency for converting and detecting this  $\gamma$ -ray which was more difficult to evaluate. De Wire and Silverman <sup>26)</sup> estimated this factor experimentally, by doing the experiment at one angle, both with and without a  $\gamma$ -coincidence with the recoil deuteron; assuming, of course, that in the latter case all deuterons

in the required energy range in the  $CD_2 - CH_2$  difference came from elastic  $\pi^0$  production from deuteron. Baron et. al. measured experimentally, the efficiency of the telescope for monoenergetic electrons of various energies, and then calculated the  $\gamma$ -ray efficiency from the statistical calculations of shower production process for  $\gamma$ 's and electrons.<sup>30)</sup> Possible contribution to the observed deuteron recoils from nuclear Compton effect, was estimated to be small in either case.

The main problem in the experiment, was however, the separation of the deuterons from protons produced by various photodisintegration, as well as inelastic pion production processes. This was done by a simultaneous measurement of two different dynamical parameters of the particles. Wolfe et. al. and Baron et.al. measured the  $dE/dx$  of the particles in a thin scintillator through which they passed, and the residual energy in a thick crystal, which stopped them.

Since

$$E \cdot \frac{dE}{dx} \sim k M^{0.8} Z^2 E^{0.2} \quad (9)$$

where k is a constant of proportionality, differentiation between particles of different mass and charge was possible. The method is a fairly standard one in high energy nuclear physics and has been applied by various workers to different problems.<sup>31,32)</sup> Davis and Corson<sup>28)</sup> used a magnet to define the momentum of the particle and used the specific ionization

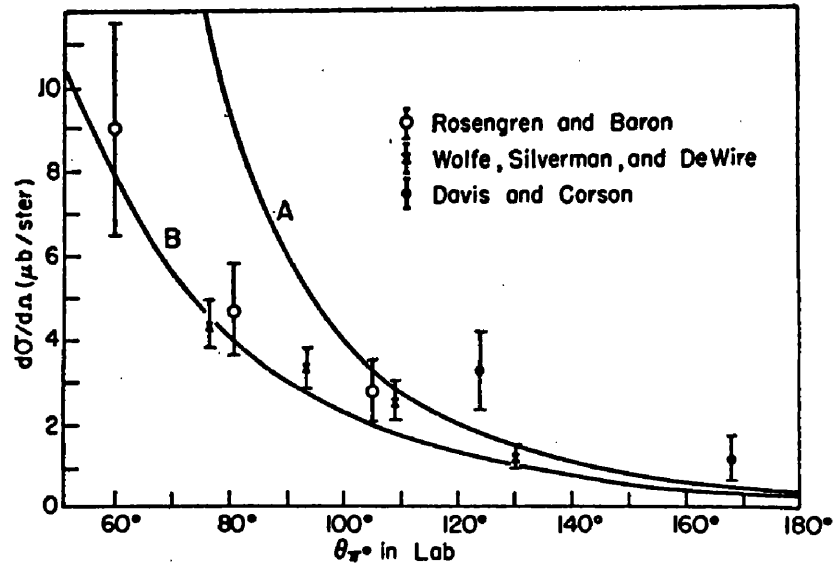


Fig.III. Angular distribution of  $\pi^0$ 's from the reaction  $\gamma + D \rightarrow \pi^0 + D$  at a mean  $E_\gamma = 280$  Mev. Curve A is based upon the impulse approximation, curve B includes multiple scattering corrections as well.

as measured by grain-densities in nuclear emulsions to distinguish between protons, deuterons and alphas.

The results of these workers are shown in Fig. III, together with theoretical curves calculated by Chappelear and Brueckner<sup>33)</sup>. They are based on Chew's impulse approximation theory (discussed earlier), and assume that the production amplitudes from neutrons and protons are the same, both in magnitude and phase, which is to be expected from charge independence hypothesis; i.e.  $\vec{K}_N = \vec{K}_P$  and  $L_N = L_P$ , (neglecting nucleon recoil effects, of course). They also assume that  $\pi^0$  production at a single nucleon proceeds only through state of  $J = 3/2$ ,  $T = 3/2$  by magnetic dipole absorption of the incident  $\gamma$ -ray. The lower curve takes into account the final state meson-nucleon interaction or what may be called the multiple scattering of the outgoing meson. The normalization for both curves were obtained from experimental data of Silverman and Stearns<sup>9)</sup> on  $\pi^0$ 's from hydrogen.

These are, however, consistently lower, by about 40% than later and more accurate measurements<sup>14,16)</sup>.

In spite of this, and the fact that there is 25% uncertainty in the absolute cross-section scale for the experimental results, because of uncertainty in estimating the  $\gamma$ -ray detector efficiency, etc, the agreement between experiment, and the corrected form of impulse approximation

seems to be reasonably good for the case of the deuteron. On the other hand if one had assumed  $\vec{K}_N = -\vec{K}_P$ , and  $L_N = -L_P$ , the calculated cross-section would have been down by a factor  $\sim 28$  over the experimentally observed values. Thus, constructive rather than destructive interference of the meson waves emitted from protons and neutrons is definitely suggested by the results of this experiment.

- 10 -

## Section (C) Photoproduction of Neutral Pions from Helium.

After having studied the fundamental photoproduction mechanism from a single nucleon from the hydrogen experiments, and having verified, at least qualitatively, the predictions of charge independence hypothesis as applied to photoproduction from the deuteron experiments, the natural and logical step would be to extend the investigation to the analogous process in Helium, i.e. to study the process  $\gamma + \text{He}^4 \rightarrow \pi^0 + \text{He}^4$  to find out how far the simple assumptions of the impulse approximation are valid in the case of the slightly more complex nucleus of Helium. In fact, there are quite a few reasons for suspecting considerable departure from this simple theory.

(i) Firstly, the helium nucleus is a very tightly bound structure with a binding energy of 28 MeV, compared with 2.2 MeV of the deuteron. This strong nuclear binding may alter the basic character of photoproduction at a single nucleon inside the nucleus into something quite different from that at a free nucleon. For the basic "impulse assumption", viz the collision time is small compared to the period of the nuclear system, is not strictly true, especially near threshold, and therefore, the neglect of the inter-nucleonic potential during the decisive phase of the interaction is no longer justified. This point is discussed in some detail by Chew and Wick<sup>34)</sup>.

(ii) Secondly, since the  $\alpha$ -particle is much more

compact in linear dimensions than the deuteron, the condition that the mean free path of the outgoing particle inside the nucleus is large, compared to the overall dimensions of the target is not true. Or in other words, multiple scattering of the meson may be expected to play a greater part, especially in energy regions where the meson-nucleon scattering cross-section is comparable to the cross-sectional area of the  $\alpha$ -particle.

Therefore, an experimental investigation of the reaction can be expected to throw light on three different aspects of the problem:-

(i) The validity of the impulse approximation as applied to photoproduction from a tightly bound nucleus,

(ii) The choice of a suitable wave function to represent the internal structure of the  $\alpha$ -particle,

(iii) The role of multiple scattering effects in modifying the cross-sections.

The reason for the choice of helium as a complex nucleus is perhaps obvious. With high  $Z$ -nuclei like  $\text{Ca}$ , strong meson absorption within the nuclear core is likely to complicate the results. The photoproduction process might even be restricted to the outer surface of the nucleus, as has been assumed by Butler<sup>35)</sup> from the observed  $A^{2/3}$  law for total photoproduction. Moreover, helium is about the limit up to which one can use proper nuclear wave function without complicating the calculations too much, rather than

resort to an independent particle model of the nucleus. Calculations based on the latter have also been performed <sup>36)</sup>, but are likely to be less reliable.

Experimental work in this field has been done by two groups so far, using different methods:-

(i) Measurements involving the  $\pi^0$  by the detection of one of both of its decay  $\gamma$ 's. This has the disadvantage that except near threshold, it involves the separation of the  $\pi^0$ 's produced by the elastic process from those produced inelastically. Also, it is extremely difficult to determine the angular and energy distribution of the initially produced  $\pi^0$ 's from a measurement of the direction of the  $\gamma$ 's alone.

(ii) Detection of the recoiling  $\alpha$ -particle.

Goldwasser, Koester and Mills<sup>37)</sup> have used the first method, using an experimental set-up similar to that used by Steinberger<sup>1,2)</sup> et.al. in their pioneering measurements on  $\pi^0$  production from carbon and hydrogen. They had two  $\gamma$ -ray telescopes looking at a 3" diameter cylindrical target of liquid helium. The plane of the telescopes and the target, which defined the plane of the outgoing meson, made an angle of  $80^\circ$  to the  $\gamma$ -ray beam. The coincidence counting rate from the telescopes was plotted for various angles between them ranging from  $180^\circ$  to  $90^\circ$ , and for different peak energies of the bremsstrahlung varying between 150 and 190 MeV.

As Steinberger et.al. have shown, the angle between the telescopes alone, serves as a non-unique measure of the meson energy; for the kinematics of the  $\pi^0$  decay strongly favour the emission of two  $\gamma$ -rays of near equal energy at

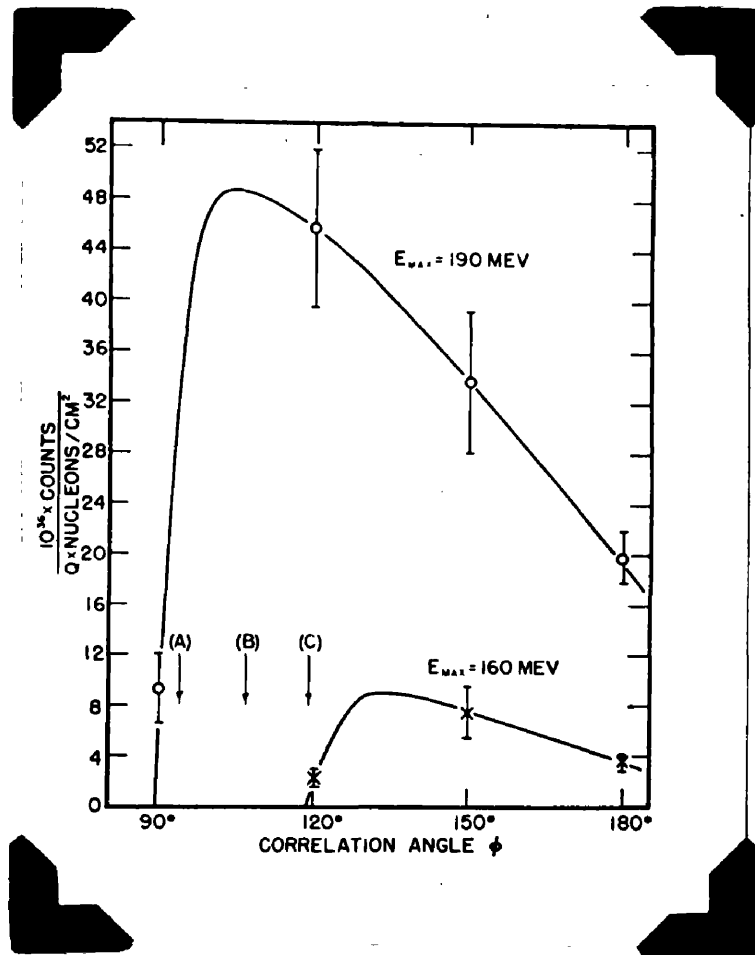


Fig.IV. Counting rates of  $\gamma$ -ray pairs from helium (Goldwasser et. al.) as a function of the angle  $\phi$  between the telescope axes. Arrows indicate minimum angles possible for (A) elastic production at 190 Mev; (B) inelastic production at 190 Mev; (C) elastic production at 160 Mev. Inelastic production is negligible at 160 Mev. Curves are arbitrarily drawn through the experimental points.

an angle close to the minimum value  $\theta = 2 \sin^{-1} E_0/E$  (10)

where  $E_0$  = rest energy of the  $\pi^0$

$E$  = its total energy

Goldwasser et.al's results (Fig. IV) show, that

(i) elastic  $\pi^0$  production definitely occurs in Helium near threshold, for with a peak beam energy of 160 MeV, there can be negligible inelastic production, the lowest threshold for that being 158 MeV. In fact, finite counting rates were observed even at 150 and 155 MeV.

(ii) even at 190 MeV, when both elastic and inelastic processes might be expected to contribute, the elastic process is predominant; since of the two minimum correlation angles  $\phi_c$ , dynamically permissible for the two processes, elastic and inelastic, the former fits the experimental data far better.

The authors also measured the coincidence counting rates from hydrogen with the same set-up for various peak  $\gamma$  ray energies from 150 to 190 MeV. In order to compare the data with those from helium, they plotted the counting rates normalised / equivalent quantum and / nucleon /  $\text{cm}^2$  against the maximum centre-of-mass kinetic energy of the  $\pi^0$  in the two cases. The dynamics of the elastic process  $\gamma + \text{He}^4 \rightarrow \pi^0 + \text{He}^4$  was used in case of helium, and all events assumed to be elastic. The results are shown in Fig. V.

They are claimed to indicate roughly equal efficiency / nucleon for elastic  $\pi^0$  production from hydrogen and helium in the energy region investigated.

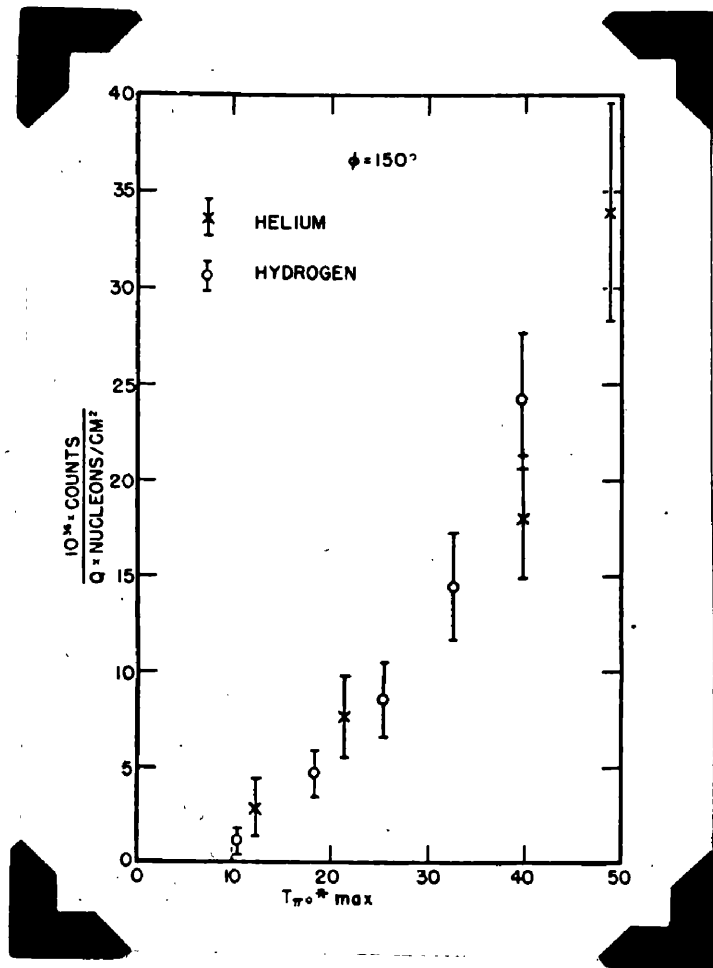


Fig.V. Counting rates of  $\gamma$ -ray pairs from helium and hydrogen plotted against maximum kinetic energy in the c.m. system corresponding to  $E_{max}$  of the betatron radiation. For helium, the dynamics of the elastic process have been used.

Goldwasser and Koester<sup>38)</sup> have also made preliminary report of some work on the same problem, using a single  $\gamma$ -ray telescope counting  $\gamma$ 's from hydrogen and helium at  $84^\circ$  in the laboratory at energies between threshold and 300 MeV. The method and the analysis are probably similar to that used by Koester and Mills<sup>19)</sup> in their work with hydrogen. It has the advantage of a higher yield than the double coincidence method. But it does not permit a determination of either meson energy, or angle, and hence the initiating photon energy is also unknown. Hence the "photon difference" method had to be used by performing mutual subtractions on runs with peak energy of the bremsstrahlung raised in successive steps of 10 MeV. Also, as has been discussed earlier (page 4), the single telescope performs an integration over mesons distributed over a wide range of laboratory angles. The authors, however, claim that as a result of the weighting of solid angle factors etc., the results should be fairly representative of the  $90^\circ$  differential cross-section. The problem of separating the "elastic" from the "inelastic"  $\pi^0$ 's is also involved.

The report is very vague, and there seems to be considerable inconsistency. The ratio of the ( $\gamma\pi^0$ ) cross-section from helium to that from hydrogen is claimed to lie between 1.0 and 0.5 in the energy range from threshold to 300 MeV, but it is not quite clear whether this is a ratio of cross-sections per nucleus, or per nucleon. In case it

is the latter, which seems probable from the general trend of the discussion, it is difficult to understand the last statement in their paper to the effect, that De Saussure and Osborne's results (to be discussed shortly) are five to ten times larger than that found in their work. This could be possibly true near threshold, but certainly not at higher energies. On the other hand, if one assumes that this ratio of 1.0 to 0.5, refers to cross-section/nucleus, then their results are certainly down by an order of magnitude over De Saussure and Osborne's results.

Apart from the fact, that the double  $\gamma$ -ray method had proved conclusively the existence of the elastic  $\pi^0$  production process from Helium, these measurements are not really of any quantitative significance. Except near threshold, they involve separation of  $\pi^0$ 's produced by the elastic process from those produced inelastically. The practice of comparing cross-sections from hydrogen and helium, and to talk of efficiency of production per nucleon is rather misleading. For, for the comparison to be really valid, it has got to be made at the same centre-of-mass energies of both photon as well as meson in the two cases, which is kinematically impossible.

The alternative, and far more conclusive method of measuring the angle and energy of the recoiling  $\alpha$ -particle has been used by De Saussure and Osborne<sup>39)</sup> of M.I.T. They bombarded a target of helium gas at 1 atmospheric pressure with 350 MeV bremsstrahlung beam, and detected the helium

nuclei in nuclear emulsions at all laboratory angles from  $0^\circ$  to  $160^\circ$ . The main problem of the experiment was, as in the case of the analogous process in deuterium, to separate the  $\text{He}^4$ 's from the  $\text{He}^3$ 's, produced in reactions, such as,



and also from singly charged particles like protons, deuterons and tritons arising from various photodisintegration processes. Distinction between singly and doubly charged particles was easily done by grain-density measurements. The  $\text{He}^3$ 's however, could not be separated from the  $\text{He}^4$ 's. Of the various reactions (11) to (13), which can contribute to the  $\text{He}^3$  yield, (11) is a two-body process, and hence its kinematics can be calculated exactly. It can be shown that all the  $\text{He}^3$ 's of energy and angle with respect to the bremsstrahlung beam, which can be confused with  $\text{He}^4$ 's from the elastic  $\pi^0$  process, are produced by photons of energy  $< 150$  MeV, which is below the meson threshold. Hence their contribution can be eliminated by a subtraction technique. De Saussure and Osborne performed a separate run with the peak energy of the machine reduced to 150 MeV, and found that the angular distribution of the  $\text{He}^3$ 's was roughly symmetric about  $90^\circ$  in the laboratory. They used this information (private communication, not clear from

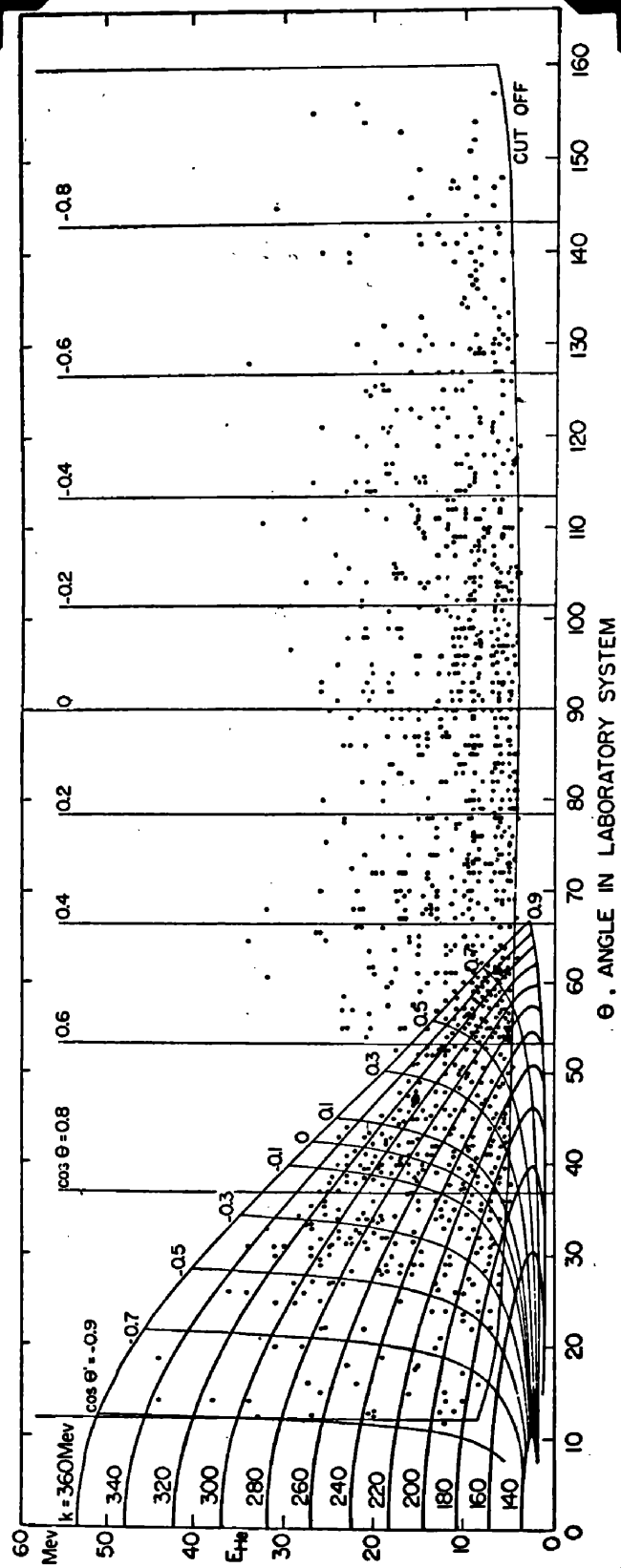


Fig. VI. Plot of events in a high energy run of De Saussure and Osborne.

Each dot represents a recoiling helium nucleus plotted with respect to its angle in the laboratory system, and its energy determined from its total range. The superimposed lines give the energy of the photon responsible and the cosine of the meson c.m. angle. The vertical lines are at equal  $\cos \theta$  intervals in the laboratory system. The cut-off represents the lower limit of observable tracks.

24

the paper) to subtract the  $\text{He}^3$  background from the high energy runs, since the maximum angle dynamically permissible for the recoiling  $\text{He}^4$  particle from the elastic  $\pi^0$  process was only  $70^\circ$ . Therefore, all recoil tracks at laboratory angles greater than  $90^\circ$  must have been due to  $\text{He}^3$ 's. Fig. VI illustrates this very clearly.

This procedure still cannot eliminate the contribution of  $\text{He}^3$ 's from the inelastic processes (12) and (13). Being three-body processes it is impossible to predict exactly the dynamical variables involved. But it can be argued that since  $\text{He}^3$  is the most massive of the three outgoing particles, it will acquire the least amount of recoil energy, maybe of the order of a few MeV, and hence would normally have been stopped in the target gas before reaching the plates. This is true, if either we assume that the  $\text{He}^3$  sits as a spectator during the interaction, or if the outgoing particles share their energy in such a way as to occupy the largest possible volume in phase-space. De Saussure and Osborne completely ignored their contributions, presumably because that was the best they could have done.

From the preceding review, it will be clear that no really reliable and quantitative measurements existed in this field at the time of embarking upon the present research work. The shortcomings of the  $\gamma$ -ray method have already been discussed. The plate work, though more detailed, and quantitative, in so far as it gave absolute differential

cross-sections at different angles and energies, was based on a subtraction technique, and involved rather questionable assumptions. In order to do this experiment really well, some means of distinguishing between the recoiling He<sup>3</sup> and He<sup>4</sup> particles had to be devised. This was done in a special type of gridded ionization chamber, which essentially measured the  $\frac{dE}{dx}$  and "E" of the particles at the same time.

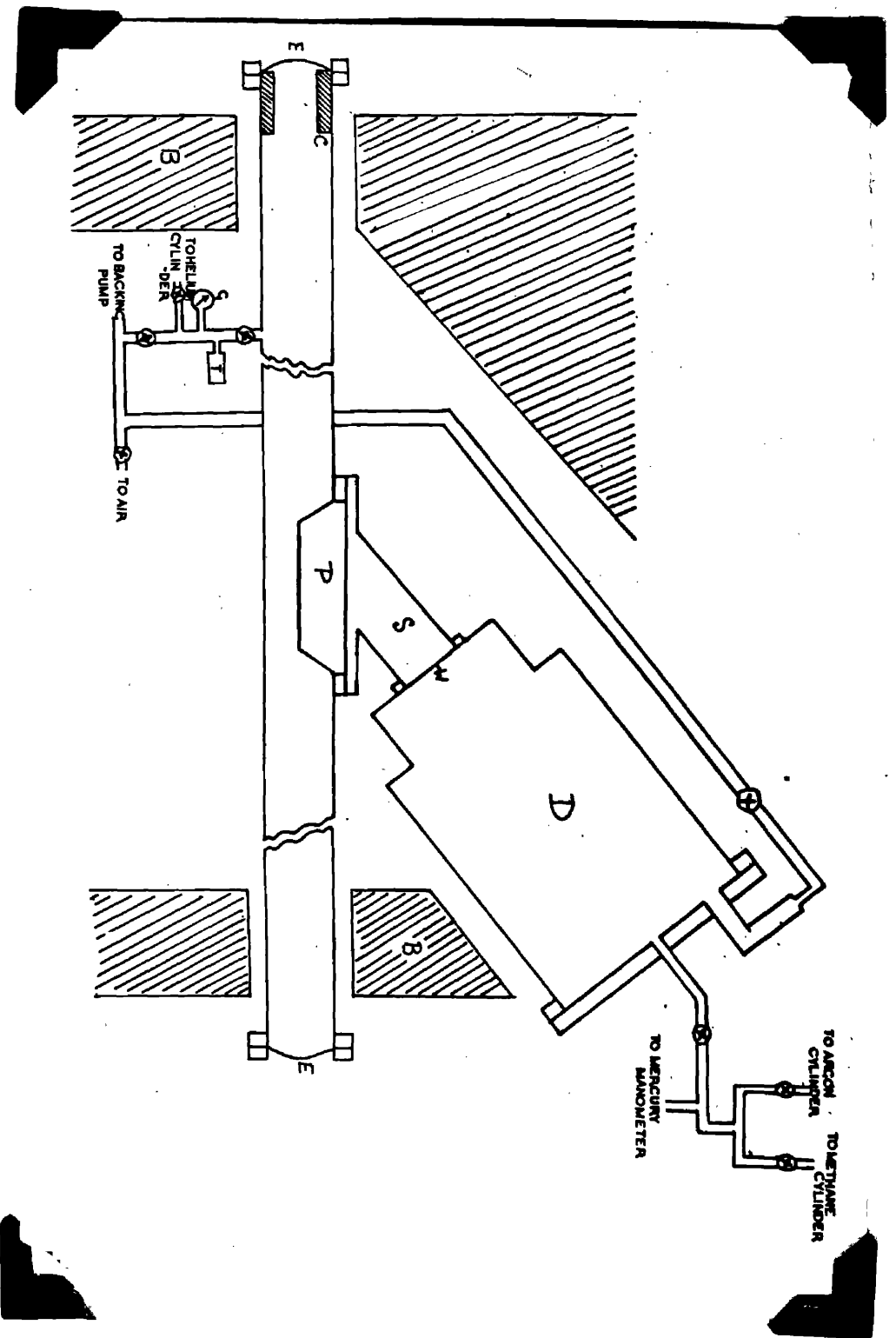


Fig. VII. Schematic view of the apparatus. The drawing is not to scale.  
 D= Detecting chamber; W = '0005" Melinex window; E = 007" Mylar window;  
 P = exit port for the particles; S = inter-changeable side-arm; C = lead  
 collimator; B = lead shielding; T = thermo-couple gauge; G = Bourdillon  
 gauge.

CHAPTER II - DESCRIPTION OF THE APPARATUS.

Section (A) The Target.

Some sort of a gas target had to be used in this experiment, because it involved a measurement of the recoil energy of the densely ionizing  $\alpha$ -particles, and self-absorption within the target material set a limit to the minimum detectable energy which in its turn tended to limit the target density. In choosing the target pressure, a compromise had to be made, therefore, between counting rate, and the range of the energy spectrum of the  $^4\text{He}$ 's that was investigated at a particular angle. It was thus found possible to explore regions of the excitation curve nearer threshold in the case of forward angles, when the recoil momentum was comparatively higher, than in the case of the larger angles.

Fig. VII shows the general layout of the apparatus. The target was a cylindrical brass pipe 2" internal diameter, filled with normal medical grade Helium gas ( ) to a pressure of 2 to 5 atmospheres. The original length was 26", but two extension pipes, each 16" long, were later fitted to the two ends so as to keep the end windows as far removed as possible from the actual detecting system D. For, even though the windows were made of Mylar only 0.007" thick, a considerable shower of high energy electrons was produced by the  $\gamma$ -ray beam on hitting them, and the detector

had to be shielded from this background by piles of lead bricks B. The central section of the target pipe had an opening P at the side, which served as an exit port for the particles, and a series of separate interchangeable sidearms S, could be bolted on to a rectangular flange on the main pipe, so as to look at particles emerging through the port at different angles to the beam. Of course, it was possible in this way only to look at one angle at a time. A collimator C, made of parallel vanes of copper with their planes at right angles to that of the diagram was placed in S, so as to limit the angle of the recoiling particles to some acceptable directions (in which they did not hit the electrodes inside the detector D). The whole arm S was evidently filled with Helium gas to the same pressure as the target, and since the recoiling particles had to traverse this pipe before they entered the actual detecting chamber, it evidently represented a dead space, the path length inside which had to be minimised. The limit was imposed by purely geometrical considerations, viz, the closest possible proximity of the detector D to the target pipe. In actual practice, the equivalent path length varied in the range 24 to 126 cm ( at 1 atmosphere pressure in Helium) between the angles  $50^{\circ}$  and  $20^{\circ}$ , and the energy losses ranged from 1.3 to 7 MeV. The following table gives the exact figures for different angles.

Table II. Energy loss in the dead space inside the target.

Angle	Mean Path Length	Pressure	Energy Loss	
			$\Delta E_{\max}$	$\Delta E_{\min}$
20°	29 cm	4 <sup>1</sup> / <sub>3</sub> Ats.	7.0 MeV	4.8 MeV
		2½ "	5.5 "	3.7 "
30°	19 cm	3½ "	4.1 "	2.7 "
40°	17 "	2½ "	3.7 "	2.2 "
50°	12 "	2 "	2.3 "	1.3 "

The whole pipe was evacuated by means of a backing pump to pressures of the order of  $10^{-3}$  mm of Hg as ready by the thermocouple gauge T, flushed several times with helium, and finally filled to the required pressure above atmospheric, which was measured by the Bourdillon gauge G. However, as there was a thin window W separating the gases in the target and the detector, which could only stand up to a maximum pressure difference of 1 atmosphere, acting one way only (target side at higher pressure), great care had to be taken in filling the system. Often this had to be done in several instalments, alternately raising the pressures in the target and the detector.

The whole assembly was mounted on a metal framework, so that the pipe was horizontal, and at the correct height ( 4' 5") from the floor for the  $\gamma$ -ray beam to pass through its length without hitting the wall. The alignment, which

was always a tedious affair, was done in the first instance visually, by looking through the transparent mylar windows, and this was finally checked by taking X-ray pictures of both the front and the rear ends with cross-wires mounted on them. C was an annular lead collar  $1\frac{1}{4}$ " internal diameter, to cut out the soft part of the beam and let only the hard core through. This had a mean diameter of 1", and an angular divergence of  $\frac{1}{4}$ "/metre at the position of the target.

Section (B) The Detecting System.

(i) Early stages. The crux of the experiment, as has already been pointed out, was the separation of the  $\text{He}^4$ 's from the  $\text{He}^3$ 's, both of a continuous energy spectrum ranging from about 10 to 30 MeV. The problem was essentially similar to that of separating deuterons from protons in the analogous reaction  $\gamma + \text{D} \longrightarrow \pi^0 + \text{D}$  which has been discussed earlier (page 13). The only difference was that it was much more difficult, because the mass ratio was only 4 : 3, instead of 2 : 1. Magnetic analysis together with energy selection, might, on first thought be expected to yield the best discrimination. But the method was actually both cumbersome and inefficient, partly because of the difficulty of bending high energy Helium nuclei into sizeable trajectories, and partly because of the fact, that owing to the large intrinsic dispersion of such a device, one could only look at a very narrow part of the energy spectrum at a time; which meant in this case, absurdly low counting rates. So it was decided to use  $\frac{dE}{dx}$  and "E" measurement as in the deuteron case. The choice of some sort of a gas counter for the  $\frac{dE}{dx}$  measurement was obvious, as an extremely thin scintillator would be required otherwise. Thus a 15 MeV  $\alpha$ -particle would lose about 5 MeV in passing through .003" of plastic scintillator.

51

In the early stages of the experiment, the detector consisted of a parallel plate gridded ionization chamber, followed by a plastic scintillator detector. The chamber and the target formed parts of an intercommunicating system filled with the same gas to the same pressure, thus providing a direct windowless path for the recoiling nuclei from their point of production to the detecting volume. However, the idea of using Helium as a chamber gas had to be abandoned eventually, partly because of gas poisoning effects, and partly because of long collection times of the electrons, observed at the available values of  $X/p$  (field strength/pressure). The latter effect was, however, anticipated right from the beginning.

By this time, quite strong and vacuum tight, yet thin windows of "Melinex" were available, and it was decided to replace the helium in the chamber by a standard mixture of 90% Argon and 10% Methane, which is normally used in ionization chamber and proportional counter work. The plastic scintillator for residual energy measurement, however, proved unsatisfactory, because of poor pulse-height resolution. Apart from the intrinsic resolution, another factor was also involved. The variation of light output with energy loss for plastic, is highly non-linear for such densely ionizing particles as helium nuclei. Thus to a first approximation, the pulse height can be taken as proportional to the range of the particle inside the crystal, rather than to its energy especially at low energies. For, the formula for specific

fluorescence, or light output/cm air equivalent <sup>40)</sup>

$$\frac{ds}{dr} = \frac{A \frac{dE}{dr}}{1 + kB \frac{dE}{dr}} \quad (14)$$

reduces to  $\frac{ds}{dr} = \text{constant}$ , in the limit of high  $\frac{dE}{dr}$

where  $kB \frac{dE}{dr} \gg 1$ . It can be easily seen that this has the effect of reducing the discrimination efficiency of the device, between He<sup>3</sup>'s and He<sup>4</sup>'s. For, if one plots  $\frac{dE}{dx}$ , against residual range, rather than against energy, the separation between the two curves for He<sup>3</sup>'s and He<sup>4</sup>'s is reduced, and the intrinsic energy resolution required to separate them is then difficult to achieve. A high background of scattered  $\gamma$ 's prevented the use of NaI, which might have been expected to yield better resolution, because its comparatively slower light emission did not allow the pulses to be clipped short enough to avoid "pile-up" trouble.

These considerations and experiences suggested, the use of some form of gas ionization counter for both " $\frac{dE}{dx}$ " and "E" measurement. Their response is linear and intrinsic resolution is high, and although the shortest pulse obtainable from these counters has much greater time duration than can be obtained from scintillation counters, the specific ionization of the doubly charged particles is so high that their detection and resolution could be expected not to be seriously affected even by the "pile-up" of counts due to relatively high fluxes of electrons and photons.

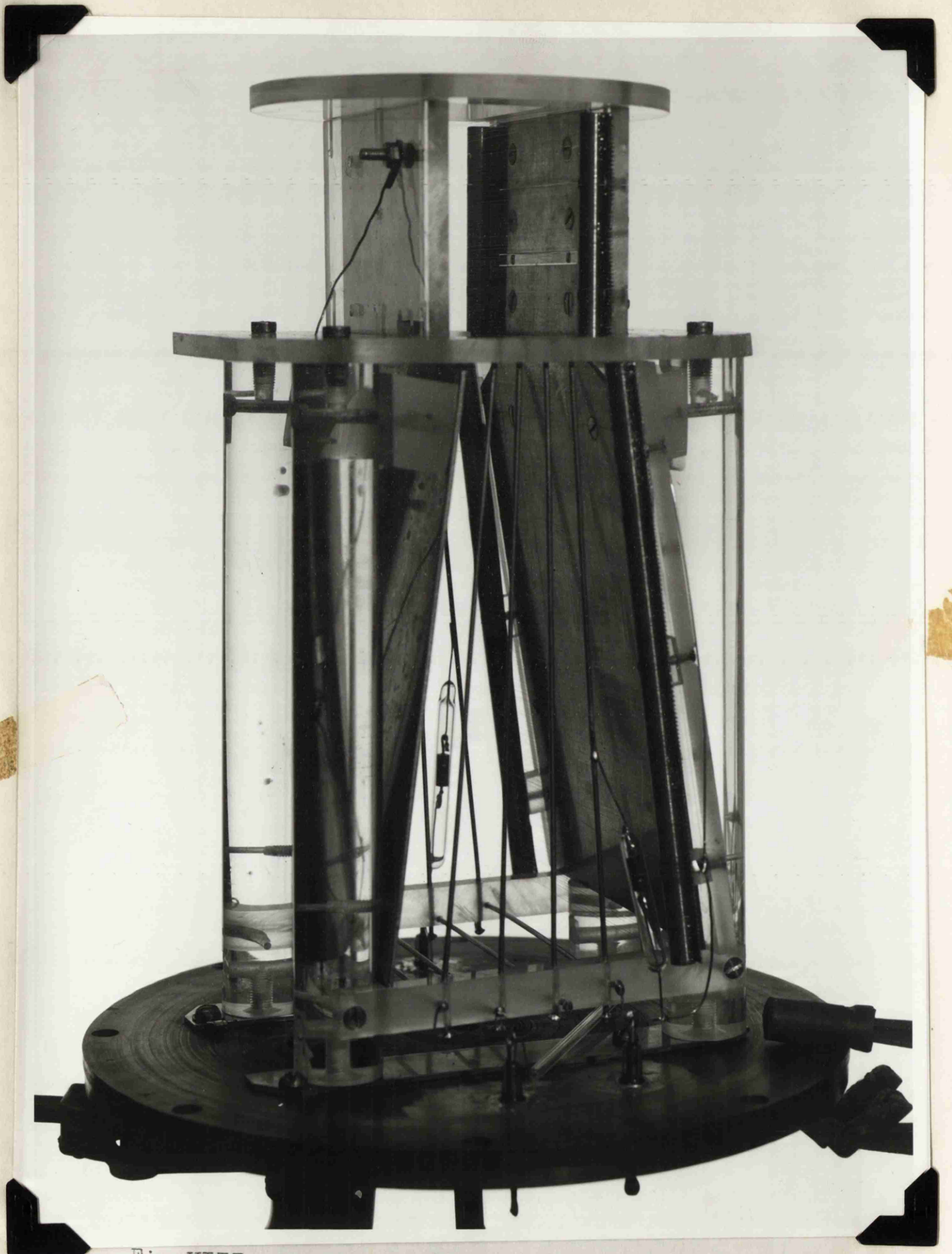


Fig.VIII. The Detector.

(ii) Final Form. After having decided on ionization chambers for both  $\frac{dE}{dx}$  and "E" measurement, there remained two possibilities. The first was to use two separate and completely independent chambers. This, though convenient from several points of view entailed one serious drawback. It inevitably involved some dead space between the chambers, which was highly undesirable, since it tended to reduce the effective separation between He<sup>3</sup>'s and He<sup>4</sup>'s. The effect was very similar to that of the non-linear scintillation response from plastic, referred to in the earlier section. It also involved a reduction in acceptable solid angle, as the "E" chamber had to be extended backwards fairly far. The alternative possibility was to house both chambers within the same assembly, so as to bring their active volumes as close to each other as mechanically possible, to get the optimum efficiency for discrimination. This, however, implied a very small path length of the ionizing particle inside the  $\frac{dE}{dx}$  chamber, if the "E" chamber were not to be too bulky, since both of them had to be operated at the same gas pressure.

The photograph (Fig. VIII) and the drawing (Fig. IX) illustrate the final form of the detector. The actual dimensions chosen are also shown in Fig. IX. The two chambers had a common H.T. electrode KL, as shown, but the collector plates CD (1.9 cm long) and GH (19 cm long) were separate, and electrically insulated from each other. Parts of GH and KL were bent outwards so as to include a

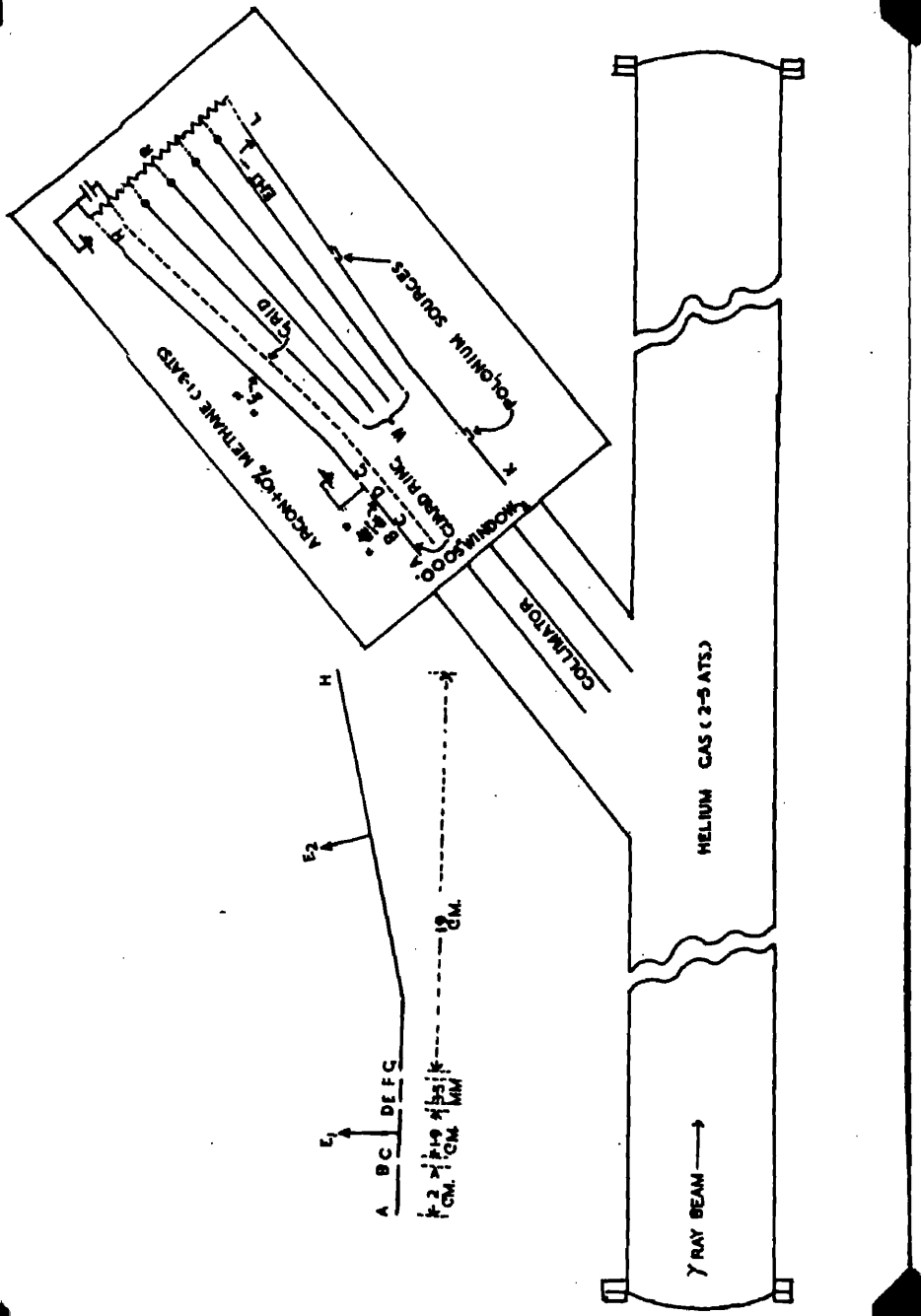


Fig. IX. The Detector: schematic view with linear dimensions.

- 54 -

reasonable solid angle of acceptance, the angular divergence being about  $15^\circ$ , the depth of the chamber being 4.5 cm at the nearer and 9.0 cm at the farther end. The gas pressure was so adjusted at each angle, that the highest energy  $\alpha$ -particle produced by the process  $\gamma + \text{He}^4 \rightarrow \pi^0 + \text{He}^4$  stopped at the far end of the chamber. Under these conditions, the plate CD collected an amount of ionization, and therefor gave a pulse height proportional to the energy lost by the particle in traversing this 1.9 cms of the chamber gas, whereas most of the residual energy, (but not the whole of it, because of the presence of the earthed strip EF, to be described later) was absorbed in the back chamber GH. These energy losses will in future be referred to as  $E_1$  and  $E_2$  respectively. So the device essentially discriminated between particles of different mass by measuring their total energy in two fragments  $E_1$  and  $E_2$ ,  $E_1$  in general being  $< E_2$ , but often of comparable magnitude, especially near the lower end of the energy spectrum. It is easily seen that the discrimination efficiency attains a maximum value when

$\frac{E_1}{E_2} \rightarrow 0$ , i.e.  $E_1$  tends to  $\frac{dE}{dx}$  in the limit.

Since the precise value of  $E_1$ , (as will be discussed later) was involved in the identification of the particle mass, and had to be calculated on the basis of the chamber geometry, it was absolutely essential to define the active volume of the  $\frac{dE}{dx}$  chamber accurately, by ensuring that the distortion of the electrostatic field near the edges was

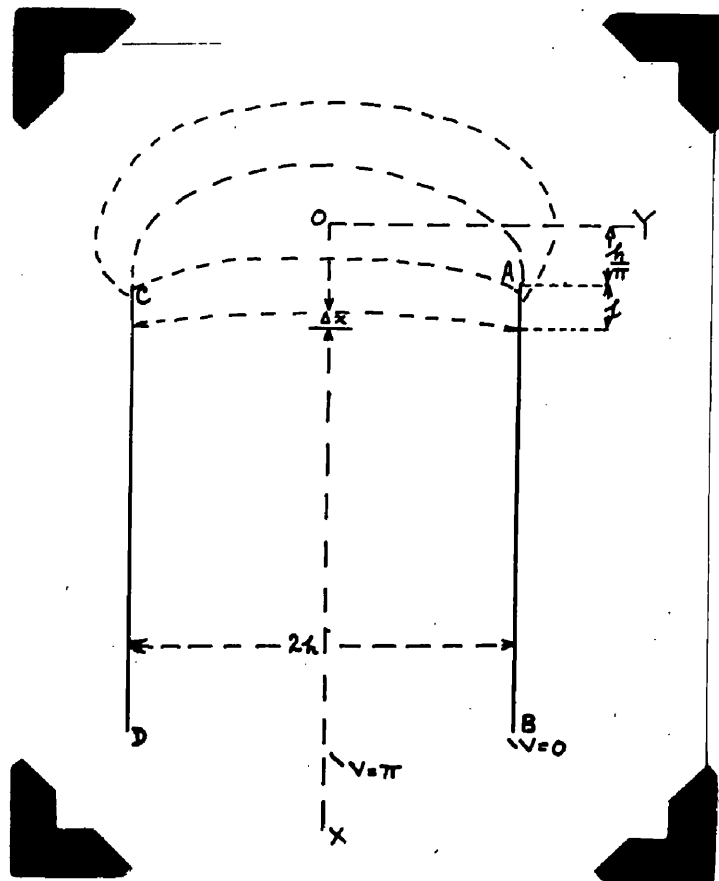


Fig.X. Diagram to illustrate the edge-effects in the parallel-plate ionisation chamber.

negligible. This was achieved by putting an earthed guardring AB 2 cm long, in front of the collector plate. This, however, increased the dead space, and the minimum length required to give an appreciably uniform field over the entire region of the collector was estimated theoretically.<sup>41</sup>

Thus in Fig. X, if AB and CD represent the two plates of the chamber at potentials 0 and  $2\pi$  respectively, and the positions of the axes of co-ordinates are chosen as in the figure, then the electrostatic field can be represented by

$$\chi = \frac{h}{\pi} (e^u \cos v - U) \quad (15)$$

$$y = \frac{h}{\pi} (e^u \sin v - U) \quad (16)$$

where the family of curves

$U = \text{Constant}$  give the lines of force

$v = \text{Constant}$  give the equipotentials.

The bulging of the line of force  $\Delta x$  along the axis, at a distance  $l$  from the edge is given by

$$\Delta x = \chi_1 - \chi_2$$

$$\text{where } \chi_1 = l + \frac{h}{\pi} = \frac{h}{\pi} (e^u - u) \quad \{ \because v=0 \} \quad (17)$$

$$\chi_2 = \frac{h}{\pi} (-e^u - u) \quad \{ \because v=\pi \} \quad (18)$$

$$\therefore \Delta x = \frac{2h}{\pi} e^u \quad (19)$$

In the present case,

$$2h = 4.5 \text{ cms} \quad l = 2 \text{ cm.}$$

$$\text{From eqn (17), } U = -3.76 \text{ and } e^u = .023$$

$$\begin{aligned} \Delta x &= \frac{4.5}{\pi} \times .023 \\ &= .033 \text{ cms.} \end{aligned}$$

Since the total length of the  $E_1$  chamber was 1.9 cms, this bulging  $< 2\%$ .

The function of the grid in front of the collector was to screen it from the inductive influence of the positive ions. In all fast chambers (microsecond pulses) employing electron collection, this is essential; otherwise the height of the output pulse tends to be a function of the position and orientation of the track of the ionizing particle inside the chamber. The screening, however, is not perfect. The calculation of the degree of shielding is complicated, and has been performed by Bunemann<sup>42)</sup>. It can be shown that the inefficiency of the grid, or the fraction of the total number of lines of force from an ionpair which finish on the collector, can be represented, in the limit of small inefficiency, by

$$\sigma \sim \frac{\xi}{2\pi C} \log \frac{\xi}{2\pi r} \quad (20)$$

$$\left(\frac{\pi r}{\xi}\right)^2 \ll \log \frac{\xi}{2\pi r} \quad (21)$$

$r$  = radius of the grid wire

$\xi$  = spacing between adjacent wires

$C$  = separation between grid and collector.

In the present case, the grid consisted of .002" diameter manganin wire wound on a screwed steel rod of pitch .05 cm and  $C$  varied between 6.5 mm at the shallow end to 1.3 cm at the deep end of the chamber.

Hence  $\left(\frac{\pi r}{\xi}\right)^2 = \frac{1}{40} = .025$

$\log \frac{\xi}{2\pi r} = 1.57$

Thus condition (21) is satisfied and

$\sigma \sim .012.$

Another important question in connection with the gridded chamber is the fraction of the electrons collected on to the grid, instead of on the collector, and so lost so far as pulse-production was concerned. If this fraction  $\lambda$  (say) were constant, this would not be very objectionable, but for some loss in absolute pulse-heights. But in general,  $\lambda$  cannot be an accurate constant, it tends to be a function of the orientation of the ionizing track, especially if the latter is formed anywhere close to the grid. Such an effect introduces an additional source of scatter in the pulse-spectrum. It was necessary, therefore, to be assured of the smallness of  $\lambda$ . The expression for  $\lambda$  is again complicated, but according to the graphs in Wilkinson's <sup>43)</sup> book, the value in the present case for  $\lambda = 0.2$ . This is assuming the same value for the electrostatic field between the grid and the collector as between the grid and the H.T. electrode, which was true in the actual case. Theory predicts an improvement in both resolution and pulse height for somewhat bigger fields in the grid collector space, compared to that between the grid and the H.T. electrode; but not much of a difference was experimentally observed over a wide range of grid potentials.

Like the earthed guard-ring AB, the function of the wire conductors W (Fig. IX), held at suitable electrostatic potentials with the help of the resistor chain R, was to maintain the required field distribution near the edges of the chamber, and thus to define its active volume. In their absence, part of the ionization would tend to be collected on to the earthed base plate and the surrounding metal cylinder container. R consisted of miniature carbon resistors, sealed inside glass tubes, so as to prevent "poisoning" of the chamber gas. The earthed strip EF was inserted between the two collector plates to reduce the capacity between them. In the absence of this plate, the value of this interelectrode capacity was  $\sim 20 \mu\mu\text{f}$ , whereas the capacity to earth, of CD, and GH separately (together with input capacities of associated amplifiers) were  $38 \mu\mu\text{f}$  and  $70 \mu\mu\text{f}$  respectively. This meant, that a large fraction of the observed pulse heights in the absence of the plate EF, would not be due to genuine electron collection but a result of capacitive pick-up from the neighbouring collector. It is easy to see, that this would have the effect of completely ruining the resolution of the apparatus. For a given value of  $E_2$ , the actual  $E_1$  values for  $\text{He}^3$ 's and  $\text{He}^4$ 's differ by say 20%. If to each of these genuine values is added a large constant contribution  $k.E_2$ , it is clear that the percentage separation is enormously reduced.

Even after the inclusion of the plate EF, the cross-coupling effect was not completely eliminated, and had to be allowed for in the analysis of the data. Its precise value was estimated in two ways; firstly by directly measuring the height of the pulse from each collector when a pulse of fixed voltage was applied to the other, and also by a direct measurement of the interelectrode capacity, which was now small, but finite (2.2 pf). The two sets of measurements were in mutual agreement. It was found, that

1 MeV lost in  $\frac{dE}{dx}$  chamber induced a pulse in the "E" chamber which was  $\cong .055$  MeV lost in it

1 MeV lost in "E" chamber induced a pulse in the  $\frac{dE}{dx}$  chamber which was  $\cong .03$  MeV lost in it.

Since in general  $E_2 > E_1$ , the effect of the pick-up was much more pronounced on the latter than on the former. A maximum contribution of up to 30% of the observed pulse height was noted for  $\text{He}^4$  particles with  $E_2 = 23$  MeV and  $E_1 = 1.6$  MeV.

Polonium sources were mounted at the back of the H.T. electrode, and the  $\alpha$ -particles emerged through small holes which partially collimated them. The pulses from the particles served to calibrate the pulse height response of the two chambers in terms of energy loss in MeV. The chamber was filled with a mixture of 90% Argon and 10% Methane to pressures of 1 to 3 atmospheres, and this gas mixture was separated from the helium in the target pipe by a "Melinex"

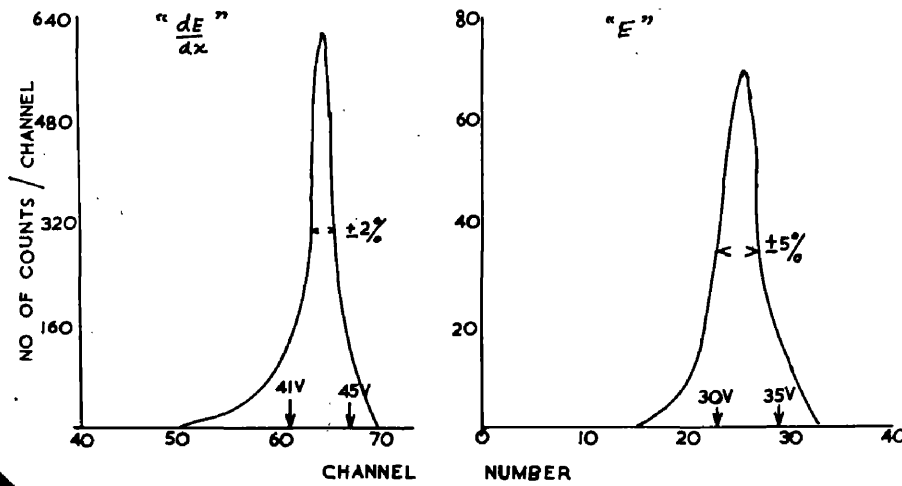


Fig.XI. Resolution of the two chambers with Polonium's

window .0005" thick ( $1.6 \text{ mg/cm}^2$ ) supported on a wire grid so as to be able to stand up to a pressure difference of 1 to 2 atmospheres. The energy loss for helium nuclei in traversing the window varied in general between .2 to .5 MeV.

All the electrodes were made of brass plates .02" thick, and were supported on a perspex structure as shown in the photograph (Fig. VIII). The latter suffered from the serious drawback of adsorbing moisture whenever exposed to air for any length of time, and this had to be completely got rid of, by leaving the whole system evacuated with  $\text{P}_2\text{O}_5$  traps inside. The presence of small amounts of water vapour leads to electron capture by negative ion-formation, and causes a diminution in observed pulse heights. The entire perspex structure supporting the electrode assembly was screwed on to the  $\frac{1}{2}$ " thick steel base plate, which had a 1" diameter hole for pumping out the air inside and a  $\frac{1}{4}$ " valve for letting the gas mixture in. 4 Kovar seals were also fixed to this plate to take out the pulses from the two collectors, and also for applying d.c. voltages to the H.T. electrode and grid respectively. The base plate itself formed the lid of the cylindrical brass container 8" diameter, (Fig. VII) which housed the whole chamber assembly, and was screwed on to the side arm of the main target pipe.

Fig. XI shows the resolution of the two chambers with Polonium  $\alpha$ 's. The "E" channel peak is seen to be twice

as broad as the  $\frac{dE}{dx}$  one. This could have several reasons. The most important one is the huge capacity of the collector and the associated amplifier (70 pf.). The signal goes down inversely as the capacity, but the most important components of the valve noise, e.g. anode current shot noise and partition noise do not. Thus signal to noise ratio deteriorates with bigger collector capacity. Part of the spread could also have been due to the awkward shape of the chamber. Some of it was almost certainly due to the source, which was not very carefully prepared and rather old. In the actual experiment, this did not matter very critically, since it was used only for the purpose of calibration. Also the average energy loss in the "E" chamber was 10 to 15 MeV, and the signal to noise, during the experiment was expected to be better than with Polonium  $\alpha$ 's. In any case, the limit of the resolution, as will be seen later was imposed by electron background in the  $\gamma$ -ray beam, rather than by the intrinsic possibilities of the detector, so that it was not considered worthwhile to go to great lengths in trying to improve these resolution curves. In fact, the resolution achieved with Polonium  $\alpha$ 's was good enough for virtually complete separation between  $He^3$ 's and  $He^4$ 's under quiet conditions (free from background).

Apart from the imperfections in the chamber itself, there was another factor affecting the resolution from the  $\frac{dE}{dx}$  channel during the actual experiment, which must be

taken into consideration. This was the intrinsic straggle in the ionization process. The theory for this has been worked out in detail by Landau <sup>44)</sup> and Symon. <sup>45)</sup>

Let  $E_m^1$  = Maximum energy transferable to an electron in a single collision

$$= \frac{2m_e c^2 \beta^2}{1 - \beta^2} \approx 2m_e c^2 \beta^2 \quad \left\{ \text{where } \beta^2 \ll 1 \right\} \quad (22)$$

where

$m_e$  = electron mass

$c$  = velocity of light

$\beta$  = velocity of the primary ionizing particle in terms of light velocity.

For a 20 MeV  $\alpha$ -particle,

$$E_m^1 = 10 \text{ KeV}$$

Then it can be shown <sup>46)</sup> that the energy distribution for particles of initial energy  $E_0$  after traversing a thin absorber  $\chi$  gms/cm<sup>2</sup> thick is a Gaussian of mean energy  $E_a$  and standard deviation  $\sigma$  given by

$$\sigma = \rho \chi^{1/2} \quad (23)$$

where  $\rho^2 = \frac{2Cm_e c^2 E_m^1}{\beta^2} \chi (1 - \beta^2/2)$  (24)

and  $C = .150 \text{ } Z^2/A$  (25)

In the limit when  $\beta^2 \ll 1$ , (24) reduces to

$$\rho^2 = (2m_e c^2)^2 C \approx .075 \text{ MeV}^2$$

This is valid if  $E_a \gg \sigma$  (26)

$$E_0 - E_a \gg \sigma \quad (27)$$

$$\sigma \gg E_m^1 \quad (28)$$

For a 20 MeV  $\alpha$ -particle, traversing a path length of 1.9 cms in Argon at 3 atmospheres, 15°C,

$$E_0 = 20 \text{ MeV}$$

$$E_0 - E_a = 1.76 \text{ MeV.}$$

$$\sigma \approx \rho x^{1/2} \approx 28 \text{ KeV independent of } E_0$$

Thus the last condition (28) was not strictly satisfied. It can be shown that in the most general case, the frequency distribution of energy losses in ionization for particles traversing a thin lamina of matter is not symmetrical about the mean value, but a skew bell-shaped figure with a sharp rise and pronounced high energy tail. This phenomenon, which makes the mean energy loss greater than the most probable energy loss is known as the Landau effect. It is due to the non-negligible probability of collisions in which the charged particle imparts appreciable kinetic energy to the electrons of the stopping material. The Landau distribution, however, approximates to the Gaussian which has been discussed, in the limit when conditions (26) - (28) are satisfied. Though condition (28) was not strictly true in the present case, a detailed calculation based on Symon's curves <sup>46)</sup> showed that the asymmetry was in fact negligible, and since the overall straggle was rather small compared to amplifier noise, ( $\sim 100$  KeV) could be safely neglected.

In the "E" chamber, however, this question did not arise, since the particle expended its entire track within the counter and the statistical fluctuations were only due to variations in the ratio of energy loss in ionization to energy loss in excitation.

Since the energy losses  $E_1$  and  $E_2$  were computed theoretically on the basis of range energy relationships of Helium nuclei in Argon, the pressure in the chamber had to be measured accurately. An accuracy of  $\pm 2\%$  was easily obtained with a closed limb mercury manometer, which was calibrated on the assumption that the air in the closed volume obeyed Boyle's Law. This calibration was checked by a direct comparison with an ordinary manometer open to the atmosphere, and the two were found to be in good agreement. Care was taken to ensure that the variation of temperature from day to day during the course of the experiment was small ( $< 2\%$ ).

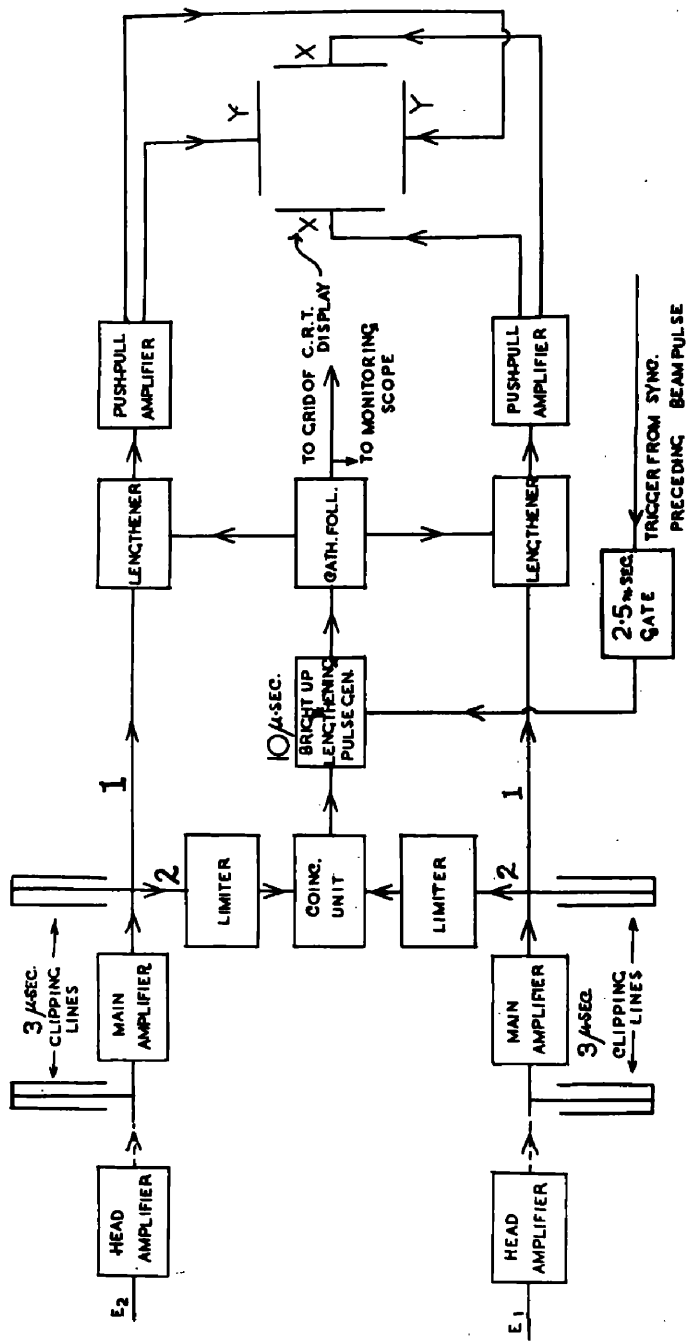


Fig. XII. Block diagram of the electronics.

(C) The Electronic Arrangement for Recording the Information.

The information from the detector was recorded electronically on the face of a cathode-ray oscillograph screen by means of an automatic plotting technique. The block diagram for this is shown in Fig. XII. Each recoiling nucleus traversing the chamber was plotted as a spot on the screen whose cartesian co-ordinates were proportional to  $E_1$  and  $E_2$  respectively.

Negative pulses from either chamber were taken out of the corresponding Kovar seal, and fed directly on to the first grid of a 1008 H.T. head amplifier (with a nominal gain of 100) through a very short length of wire, which was properly screened from stray electric and magnetic fields. Since the 1008 head amplifier used a pentode input an additional source of noise was introduced due to the partition of the anode current between the screen and the plate. The noise level (half of peak to peak value, as measured visually on a cathode-ray oscilloscope) was about 120 KeV in terms of 5.3 MeV Polonium  $\alpha$  signal height, in the " $E_1$ " and about 250 KeV in the " $E_2$ " chamber. An improvement of more than 50% was achieved in the last series of runs (at a laboratory angle of  $20^\circ$ ) by replacing the  $E_1$  head amplifier by one of the cascode type with a triode input. The overall gain was reduced because of Miller effect in the triode and hence an additional valve was needed to compensate for this loss. The basic circuit was taken from Harvey <sup>47)</sup> et.al.

The head amplifier which had a very low output impedance (of the order of a few ohms) drove a long length (25 feet) of cable from the beam room to the beam research room, one floor higher up, where the main amplifier and all the rest of the electronic equipment were kept. In order to get sharply defined spots on the screen, it was essential to shape the output of the head amplifier into square, i.e. flat-topped pulses. This was done with a lumped impedance clipping line ( $2\tau \sim 3 \mu\text{sec.}$ ) consisting of 15 sections of  $100 \mu\text{H}$  inductances in series, and  $100 \mu\text{F}$  condensers in parallel. Individual coils and condensers had to be trimmed separately so as to minimise reflections from the discontinuities between the sections. The application of a step function of voltage at one end from a pulse generator, with the far end short-circuited, produced a square pulse with a rise time  $\sim 2 \mu\text{sec.}$  and a ripple on the top whose peak to peak value was  $< 2.5\%$  of the mean pulse height. The line which had a characteristic impedance of 1 kilo ohm was matched on the cathode of a cathode follower with a series resistance of  $\sim 1 \text{ k}$ , (since the cathode follower output impedance was very low,  $\sim 100 \text{ ohms}$ ), and this pulse shaping unit was placed just before the main amplifier.

The pulses coming out of the head amplifier preceding it were negative, several millivolts high, with a rise time determined by the scatter in the transit-time of the electrons ( $\sim 0.5$  microsecond) inside the chamber, and a fall time of  $50 \mu\text{sec.}$ , (the inherent differentiating time of the amplifier), which was thus  $\gg 3 \mu\text{sec.}$ . The main amplifier was of  $1008\beta$  type, with two standard rings of 3 in series, and produced positive pulses up to 50 V high; of these, only those lying in the range 8 - 30 volts were recorded on the linear portions of the cathode ray tube screen.

The chief factor responsible for spoiling the resolution of the apparatus was the high background of electrons produced by the  $\gamma$ -ray beam. Part of it came from the end windows of the target pipe, part from the helium gas itself. A single fast electron going right through both chambers at a pressure of say 3 atmospheres, would lose about 25 keV in the front and 250 keV in the back chamber, and it was estimated that at a laboratory angle of  $20^\circ$ , on an average, some 100 individual electron pulses occurred over the period of the bremsstrahlung beam pulse lasting for about  $500 \mu\text{sec.}$  The intensity of this electron background increased with the beam intensity reaching its maximum value somewhere near the end of the  $500 \mu\text{sec.}$  interval.

Without any differentiation on the collector this would tend to build up to an enormous pile-up pulse, an effect which was greatly reduced by the 3  $\mu$ sec clipping line between the amplifiers. Even then, the pulses were observed to sit on the top of a general pile-up "pedestral", and a second clipping line of the same length was found to be very helpful in reducing this "pedestral" height. The pulse height from desired heavy particles should not, of course, have been affected by these lines.

For the best safeguard against pile-up, the clipping time had to be as short as possible. 3  $\mu$ sec. was chosen to allow for maximum possible scatter in the electron collection times from various parts of the chamber under the operating conditions of pressure and field strength, and also to allow for a small possible delay between the two channels. Another factor directly involved was the duration of the  $\gamma$ -ray beam. For a given output of photons per pulse, the amount of pile-up should be inversely proportional to the duration of this pulse. This, however, could not be increased beyond a certain maximum, round about 500  $\mu$ sec, without distorting the shape of the bremsstrahlung spectrum, especially near the top end. For, with a very extended beam, comparable in time to 5 milliseconds (which was the quarter period of the alternating magnetic field of the synchrotron) the

circulating electrons within the do-nut would not all hit the target at peak field, and would not, therefore, be monoenergetic. Also, with an experiment of this type, it would have been preferable to use a synchrotron pulsing say 50 times/sec, (as in many of the laboratories of the United States) rather than 5 times/sec as the Glasgow machine. Because in the former case for the same beam output and pulse duration, ten times fewer photons would be produced per pulse, and the pile-up reduced accordingly.

After the second clipping line, the pulses were fed simultaneously into two channels. In channel 1, they passed, first through a lengthener, and then a push-pull amplifier, before being applied to the X or Y deflection plates of the display unit. The two halves of the amplifier had each a gain of 10, and produced pulses up to 200 V amplitude and of opposite polarities. In this way the mean electrostatic potential in the region between the plates was left unaltered and the focusing of the spot on the screen was not appreciably affected. The cathode ray tube was a Vcr-97 with a blue fluorescent screen 5" in diameter, (of which only the central  $2\frac{1}{2}$ " square portion was used for the sake of linearity) and was operated with the cathode at a negative E.H.T. of 3.2 K.V.

The d.c. voltages on the X and Y plates were so adjusted that the spot, in its undeflected position was somewhere near the bottom left corner of the screen and defined the origin of the co-ordinate system. The grid of the tube was, however, normally biased beyond cut-off, so that no fluorescence actually appeared on the screen under steady conditions. It might be added here, that no commercially available cathode ray oscillograph was found to be readily adaptable to meet the requirements of this experiment, and so it was decided to build this particular unit.

In channel 2, the pulses were fed through a limiter which inverted their sign and limited them to a maximum height of 10 volts, on to the grid of a cathode coincidence unit ( $\tau \sim 10^{-7}$  sec). The ratio of the pulse height outputs of this unit with coincident and single channel inputs respectively, was 6:1. The purpose of the limiter was to ensure that a very big single pulse in one input (often due to spurious pick-up) did not give rise to an output big enough to trigger the following stage. The latter was a flip-flop which generated a 45 volt square pulse 10 *µsec.* long and its triggering level was set so that it fired only on genuine coincidences. The flip-flop pulse served a threefold function. It simultaneously lengthened the original  $E_1$  and  $E_2$  pulses from 3 to 10 *µsec.*, brightened up the spot on the cathode ray tube

display unit, and was also fed on to a monitoring scope, which was in its turn triggered by a pulse from the synchrotron. Thus a genuine recoil event occurring during the beam showed up as a big positive pulse at the proper place on the sweep.

During the actual experiment, however, it was found that spurious pulses were picked up in both the  $E_1$  and  $E_2$  channels due to huge electrical disturbances associated with the running of the synchrotron itself. These occurred at various stages in the complete cycle of operation of the machine, such as the firing of the ignitron, the pulsing of the electron-gun in the do-nut, and so on.

Such a pick-up in both channels would simulate a genuine coincidence due to the passage of a charged particle through the chamber, and would give rise to a spurious spot on the screen. Therefore, the output of the coincidence unit which triggered the "bright-up" flip-flop had to be gated with the actual  $\gamma$ -ray beam pulse. This lasted for about 500 - 800  $\mu\text{sec}$ , and a trigger from the machine preceding this pulse opened a gate for 2.5 milliseconds, which was the only time when it was possible to record events of interest on the screen. The width of the gate was chosen to allow

for possible jitter in the timing of the beam, as well as for fluctuations in its duration.

The spots on the cathode ray screen were photographed with a Cossor Scope Camera on 35 mm film. The normal running time per frame was 2 hours and it was found convenient to keep the camera shutter open all this time. The number of relevant spots per frame varied roughly between 7 and 20. At the end of each run the X and Y co-ordinate axes for the frame were located using the pulses from the Polonium  $\alpha$ -sources fixed inside the chambers. For this, the synchrotron was stopped, the 2.5 ms. gate disconnected from the bright-up pulse generator and coincidences were forced by joining the inputs of the coincidence unit. The X-axis was plotted by shorting to earth, the input of the Y-amplifier of the oscilloscope, and vice versa. The amplifier gains in each channel, had to be altered, of course, to get suitable deflections from 5.3 MeV  $\alpha$ 's, and these deflections also afforded a direct calibration of the display unit in terms of the energy losses  $E_1$  and  $E_2$  in MeV. Because of the finite resolution of the chambers, the spots, however, did not all fall on top of each other, but rather formed an extended line. The actual calibration was, therefore, done more



Fig.XIII. Photograph of the cathode-ray tube screen showing the result of a two hour run. The cluster of points near the origin represents singly charged particles, the band in the centre corresponds to the helium nuclei.

accurately by moving the film on to the next frame, and repeating the procedure with a "wobble" superimposed at right angles to the deflections produced by the Polonium pulses, so that the spots were spread out in a traverse direction and the region of maximum density could be accurately located. For any one set of runs, the calibration measurements were in sufficient agreement for their average to be taken and used throughout.

The 35 mm negative was enlarged to 6" x 7" size. A typical print is shown in Fig. XIII. The close cluster of points near the origin represents singly charged particles whose comparatively lower specific ionization keeps them widely separated from the Helium nuclei which appear as a broad band shaped roughly into a rectangular hyperbola along the centre of the frame. A minimum level of some 8 volts was required in either channel to trigger the display unit, which explains the sharp cut-off in the distribution of points near the origin. The analysis of the information contained in the central band is discussed in the subsequent chapter.

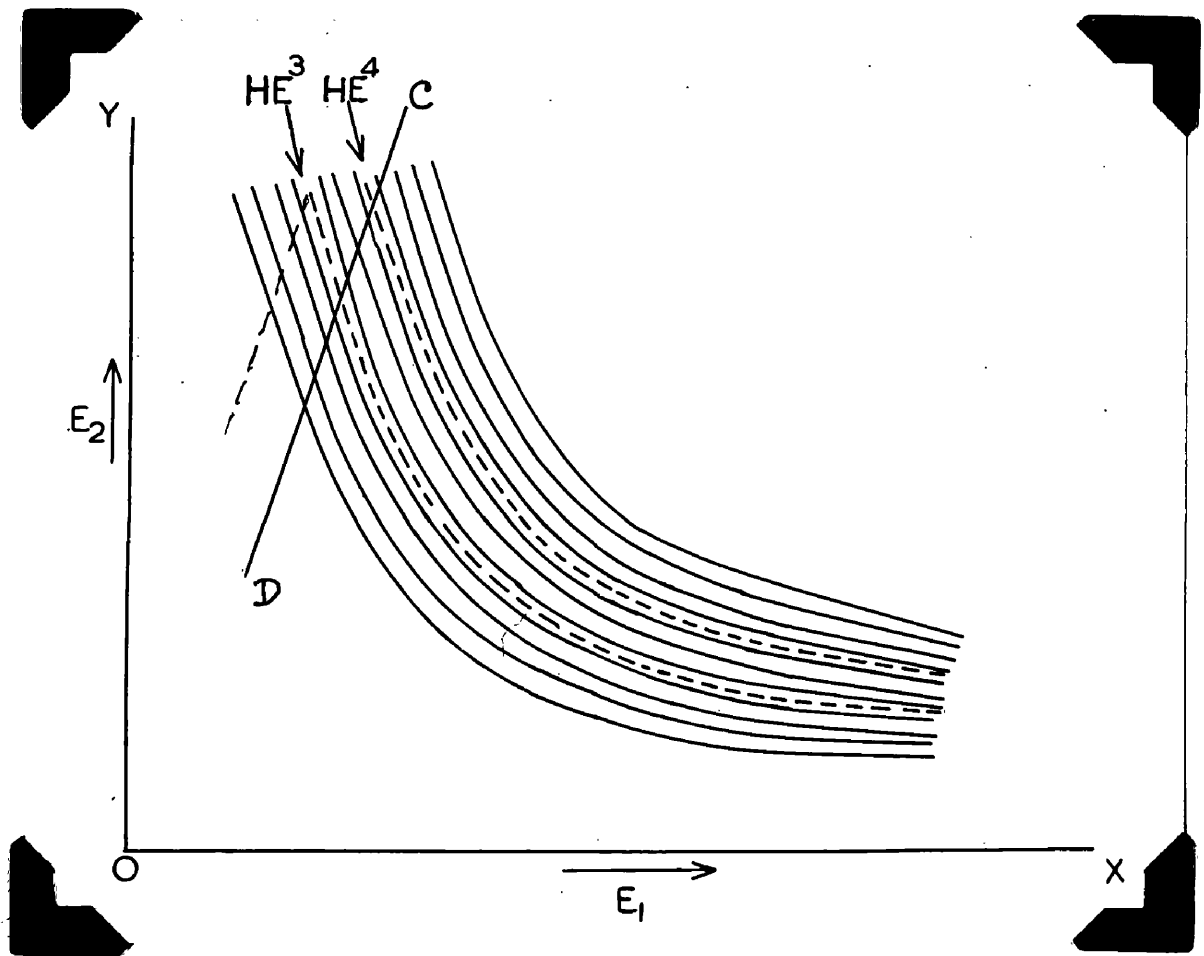


Fig.XIV. Diagram indicating the general procedure for analysing the experimental data. The dotted curves are theoretically calculated.

Chapter III - ANALYSIS OF THE DATA AND EVALUATION  
OF CROSS-SECTIONS.

Section (A) General Procedure - If the resolution of the apparatus were perfect, helium nuclei of two different masses 3 and 4 would have appeared as spots distributed along two different curves of the type shown on Fig. XIV (dotted curves). However, as the separation between the curves on an average was only about + 8% (measured along a straight line at  $45^{\circ}$  to the co-ordinate axes) the spots, as mentioned earlier, were actually smeared out into a broad band. The position of individual spots in the band, therefore, had to be compared with calculated loci to obtain the mass and energy spectrum of the particles. The calculations were done on the basis of the calibration deflections (referred to in the last chapter), the geometry of the chamber, the gas pressure and the theoretical range-energy relationship for helium nuclei in Argon. The latter was derived from the range-energy data for air given by Rich and Madey <sup>48)</sup>, the data of Bates <sup>49)</sup> being used to estimate the relative stopping powers of air and Argon, below 5 MeV.

The He<sup>4</sup> data were deduced from the published He<sup>3</sup> ones with the help of the formula.

$$R_{\text{He}^4}(E) = 4/3 R_{\text{He}^3}\left(\frac{3E}{4}\right) \quad (29)$$

$$\left(\frac{dE}{dx}\right)_{\text{He}^4} \text{ at energy } E = \left(\frac{dE}{dx}\right)_{\text{He}^3} \text{ at energy } \frac{3E}{4} \quad (30)$$

The space between the curves, and on either side of them was then divided into channels of equal width by curves which closely followed the shape of the guiding ones (Fig. XIV). The number of points within each channel was then counted separately and a histogram was thus obtained.

As has been mentioned earlier the gas pressure inside the chamber was so chosen as to stop the highest energy  $\alpha$ -particle at the far end. Some of the more energetic He<sup>3</sup>'s, however, were not stopped inside the collecting volume, and for these the (E<sub>1</sub> - E<sub>2</sub>) curve tends to fly back beyond a certain limit, as shown in Fig. XIV. Analysis was only confined to the area right of the line CD, well removed from this fly back, so that points arising out of such events did not cause any confusion.

In computing the dotted curves, the effect of the capacitive coupling between the chambers was taken

into consideration, as well as the fact that the angle between the co-ordinate axes of the display unit was not quite  $90^{\circ}$ , which is clear from Fig. XIII.

Since the whole analysis was based on these calculations it was absolutely essential to seek a direct experimental verification of their correctness . This was done in two different and independent ways which are described in the following sections.

Section (B) - Experimental Check with Polonium  
 $\alpha$ -Particles.

The chamber was disconnected from the target pipe, and the end window was closed with a brass plate having a collimated Polonium source mounted at its centre. This fired  $\alpha$ -particles into a narrow cone along the common axis of both chambers. By adjusting the gas pressure, the  $\alpha$ 's were made to stop at various points on this axis, ranging between 11 cm and 1 cm inside the "E<sub>2</sub>" chamber. Thus the energy losses E<sub>1</sub> and E<sub>2</sub> were altered, and the resulting spots on the cathode ray tube screen were photographed on the same film. 4 clusters of spots were obtained corresponding to the four different pressures used.

According to Bates <sup>49)</sup>, the average stopping power of Argon for  $\alpha$ -particles in the last 4 cm of their range at N.T.P. is 0.93 relative to air. Since a Polonium  $\alpha$ -particle of energy 5.3 MeV. has a range of 3.75 cm in air at N.T.P., this value for the relative stopping power can roughly be taken to apply in the present case. The ratio increases to a limiting value of .99 at high energies.

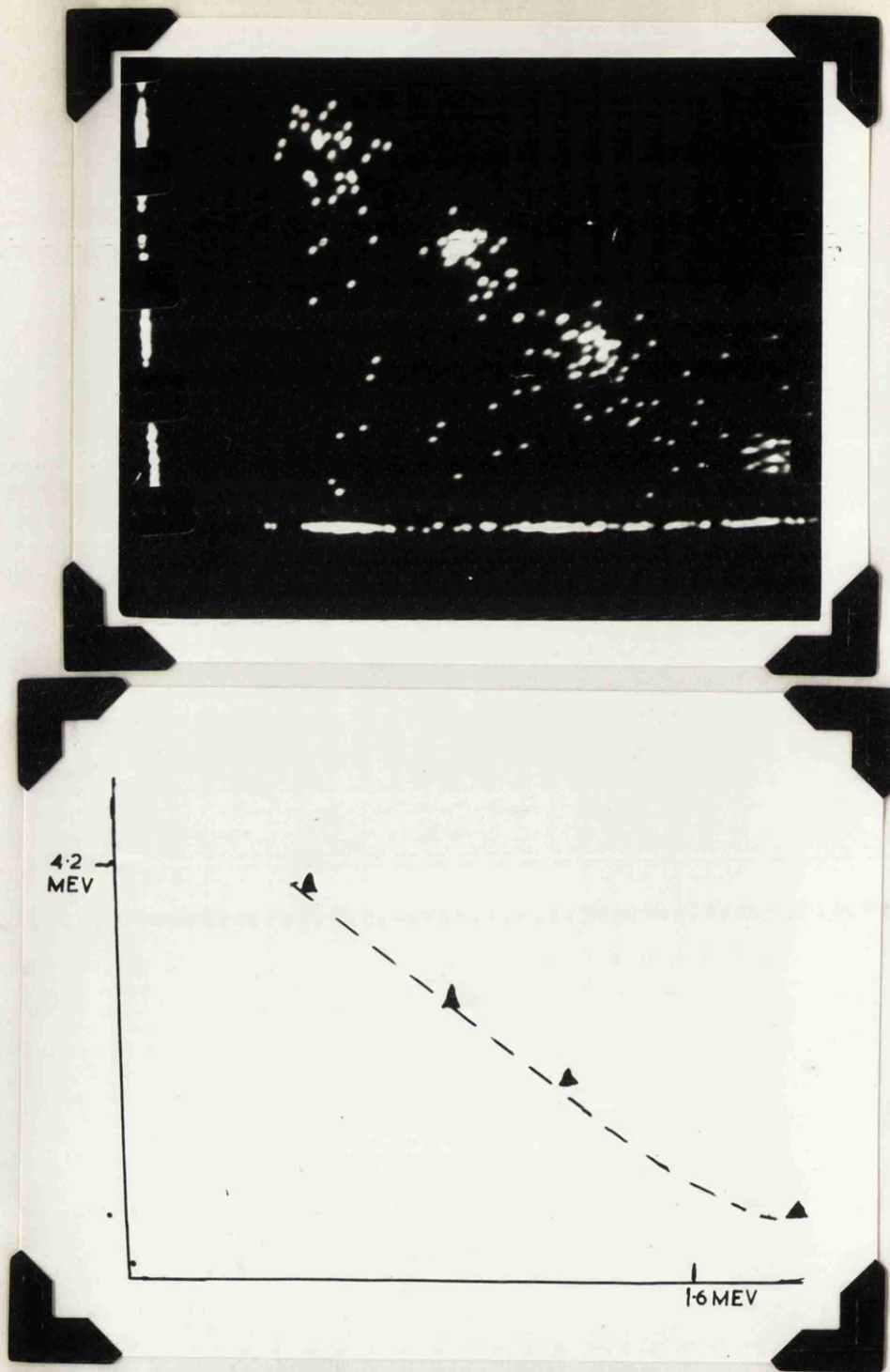
In computing E<sub>1</sub> and E<sub>2</sub>, the measured pressure inside the chamber was multiplied by a factor 0.93

to convert from Argon to air. The range-energy data for  $\alpha$ -particles in air as given by Aron<sup>50)</sup> et.al. were then used, rather than the corresponding He<sup>3</sup> values given by Rich and Madey<sup>48)</sup>, because the former gave a more detailed curve for low energies. The effect of the Methane was ignored, in the absence of a reliable way of estimating it. This, in any case is small<sup>63)</sup>. The particles traversed a total path length of 4 cms before entering "E<sub>1</sub>" chamber, and there was a dead space of 3.5 mm between the chambers.

The following table shows the values of the various parameters.

Table III Energy Loss Calculations for P<sub>0</sub>  $\alpha$  -particles fired through both chambers.

Run No.	Pressure	Range of Penetration inside "E <sub>2</sub> " chamber.	"Corrected" E <sub>1</sub>	"Corrected" E <sub>2</sub>
1	44 cm of Hg	0.7 cm	1.88 + .02 = 1.90 MeV	0.65 + .10 = 0.75 MeV
2	35.6 "	2.3 cm	1.22 + .06 = 1.28 MeV	2.02 + .07 = 2.09 MeV
3	28.8 "	4.4 cm	0.85 + .09 = 0.94 MeV	2.89 + .04 = 2.93 MeV
4	17.9 "	10.9 cm	0.44 + .12 = .56 MeV	3.97 + .03 = 4.00 MeV.



Figs. XV & XVI. Comparison between observed and predicted positions of spots on the cathode-ray tube screen from Polonium  $\alpha$ -particles fired through both chambers. The dashed curve in the lower figure is the best fit through the clusters of points shown in the upper figure. The triangles represent calculated coordinates.

Fig. XV shows the actual spots. The dotted line in Fig. XVI is the best fit through them. The crosses are the experimentally calculated co-ordinates. The word "correction" refers to the contribution from capacitive pick-up. The intercepts on the co-ordinate axes are the calibration deflections from sources inside the chambers, of course, with different amplifier gain settings.

In view of the rather uncertain nature of the stopping power of the gas mixture, as also the theoretical uncertainties in the range-energy relationships at low energies, the agreement between observed and predicted positions of the spots must be regarded as excellent. It is also to be remembered, that the overall energy losses, particularly the " $E_1$ " values were very small, of the order of a fraction of an MeV. A small absolute error in estimating them, from range-energy graphs could cause a big percentage change. The agreement could be expected to be even better in the actual experiment, when the energy losses were higher.

Section (C) Experimental Check in a Run on the Beam.

In the experiment just described, all the  $\alpha$ -particles had initially the same energy. The energy losses  $E_1$  and  $E_2$  were varied artificially by altering the gas pressure. A slightly different and independent way of checking the calculations would be to keep the chamber pressure constant, and to use particles which had a continuous energy spectrum to start with. These were precisely the conditions during an actual run on the  $\gamma$ -ray beam.

As Fig. VI, page 24 shows, the maximum angle which a recoiling  $\text{He}^4$  nucleus from the reaction



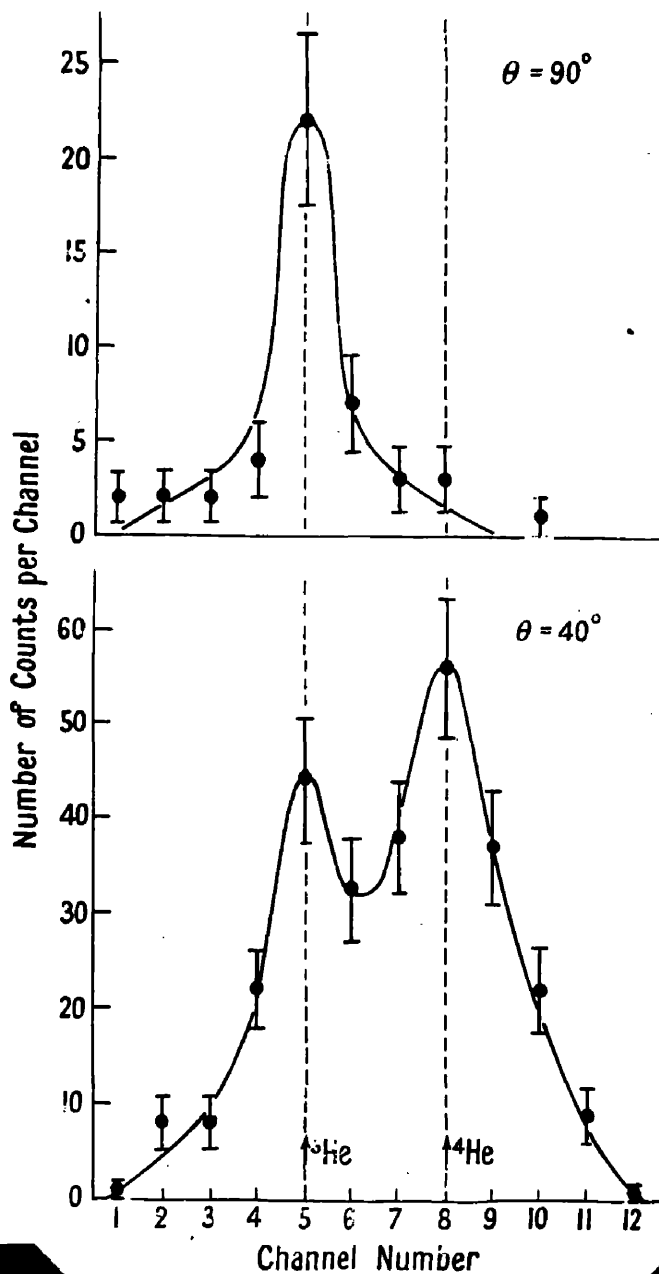
could make with the incident photon beam was  $\sim 65^\circ$  in the laboratory system, assuming a peak bremsstrahlung energy of 340 MeV. The  $\text{He}^3$ 's from the photodisintegration reaction



were, however, distributed over all possible laboratory angles from  $0^\circ$  to  $180^\circ$  and had a continuous energy spectrum. Therefore, a run on the machine at an angle

$> 66^\circ$  could be expected to provide the ideal conditions for direct experimental verification of the calculated loci for the spots on the cathode ray tube screen.

Fig. XVII shows the result of such a run at a



Figs. XVII. & XVIII. The mass spectra at  $90^\circ$  &  $40^\circ$  to the photon beam. The kinematics for the process  $\gamma + \text{He}^4 \rightarrow \pi^0 + \text{He}^4$  rule out the possibility of emission of  $\text{He}^4$ 's at  $90^\circ$ . The figures confirm the correctness of the basic analysis of the data.

laboratory angle of  $90^\circ$  (chosen because of small electron background).

The target pressure was 4 atmospheres of Helium, the chamber pressure was  $1\frac{1}{2}$  atmospheres of Argon and Methane. The energy of the  $\text{He}^3$ 's varied between 20 and 12 MeV at creation. The histogram was obtained by the method described on page 55 . (These mass spectra will in future often be referred to as histograms, though they have not actually been drawn as histograms, chiefly for the sake of showing the resolution of the apparatus).

Three conclusions could be drawn,

- (1) A single peak of  $\text{He}^3$  was obtained at the proper channel. This confirmed that the basic analysis of the data was essentially correct, the calculated curves were of the right shape and had the correct location.
- (2) The intrinsic resolution of the detector was quite good.
- (3) That the contribution of  $\text{He}^4$ 's from processes other than photoproduction such as scattering by  $\gamma$ 's or by possible neutron contamination of the beam was negligible, at least at this angle.

Fig. XVIII shows the mass spectrum of the particles at a laboratory angle of  $40^\circ$  . The chamber pressure and the amplifier gains were exactly the same as in the previous run, and the analysis was done with the same calculated loci. The  $\text{He}^4$  peak from the photoproduction

process is clear and prominent. The working of the apparatus and the soundness of the analysis was thus firmly established.

Section (D) Calculation of Cross-Sections.

The differential cross-section for the process  $\gamma + \text{He}^4 \rightarrow \pi^0 + \text{He}^4$  at a particular angle in the laboratory system was calculated from the relationship

$$\frac{d\sigma}{d\Omega} = \frac{N}{N_{\gamma} \times n \times t \times d\Omega} \quad (31)$$

where

$N$  = No. of recoil  $\text{He}^4$ 's observed

$N_{\gamma}$  = No. of photons responsible

$n$  = No. of target nuclei/c.c.

$t$  = effective target thickness

$d\Omega$  = effective solid angle of acceptance.

Of these  $N$  was obtained from the histograms just described. To evaluate  $N_{\gamma}$ , one had to measure the total integrated beam energy used over the period of the experiment, assume a shape for the bremsstrahlung spectrum and calculate the range of energies of the initiating photons from the observed range of the recoil  $\alpha$ -particle energies. This was done with the help of the reaction dynamics diagram of Fig. VI (page 24).

If  $N(E)dE$  is the number of photons in the bremsstrahlung in the energy region between  $E$ , and  $E+dE$

then

$$Q = \frac{\int_{E_0}^{E \text{ max}} N(E) dE}{E \text{ max}} \quad (32)$$

is defined as the number of equivalent quanta in the beam.

To a first approximation

$$\begin{aligned} N(E) &\propto \frac{1}{E} \\ &= \frac{K}{E} \end{aligned} \quad (33)$$

where  $k$  is a constant

$$\therefore Q = k$$

and the number of photons in the energy interval between  $E$  and  $E + \Delta E$  is just given by

$$\begin{aligned} N &= \int_E^{E + \Delta E} Q/E dE \\ &= Q \log \left( 1 + \frac{\Delta E}{E} \right) \\ &= Q \frac{\Delta E}{E} \quad \left( \text{when } \frac{\Delta E}{E} \ll 1 \right) \end{aligned} \quad (34)$$

The actual spectrum, however, deviates considerably from that predicted by the simple relation (33), especially at lower energies, and for accurate work,

the proper shape (either calculated, or measured) must be used. Eqn. (34) has only been derived to show how  $N$  and  $Q$  are roughly related to each other.

$Q$  was measured with an ionization chamber, identical with that used at Cornell <sup>51)</sup>, and in fact, their calibration was used too. The  $\gamma$ -ray beam after passing through the target pipe, went through an air filled ionization chamber, and developed a shower in copper plates  $\frac{3}{4}$ " thick inside it. The current from the chamber was integrated electronically on a capacitor, and gave a measure of the total ionization produced by the shower, and hence also of the integrated beam energy, so long as the peak energy of the bremsstrahlung and its shape remained constant. The calibration of the monitor was checked independently by measuring the yield of  $\pi^-$ -mesons from a carbon target, using known values of photoproduction cross-sections. The Cornell measurement of the bremsstrahlung spectrum was also used, which agreed essentially with that theoretically predicted by the Bethe-Heitler <sup>52)</sup> formula for a thin target.

The evaluation of  $t \cdot \Delta \Omega$  however, was a rather tedious affair. For, the target thickness was not well defined, nor was the laboratory angle  $\theta$ , of the



recoiling particle. Owing to the finite extensions of the target, and the detector,  $\theta$  varied over a somewhat wide range around the mean value.  $\theta_m$ , defined by the geometrical axes of the target pipe and the side-arm respectively. "t" was, in general, a function of  $\theta$ , not necessarily a smooth or continuous function, because of the somewhat arbitrary restrictions imposed upon the direction of the outgoing particle by the collimator (to prevent it from hitting any of the electrodes of the chamber, as discussed earlier)  $t \cdot \Delta\Omega$ , therefore, had to be evaluated by graphical integration.

Fig. XIX illustrates the position. It represents the sectional view in a horizontal plane. AB is the geometric axis of the target pipe from which all recoil trajectories were assumed to originate. (This, however, was not strictly true, since the beam had a finite cross-sectional area, 1" in diameter). CD is the width of the rectangular aperture (closed with a "Melinex" window) through which the particle entered the detector. Let its height in the vertical direction, i.e. in a plane at right angles to that of the diagram be  $l$ . QRST represents the collimator.

Thus, for a point P on the axis AB, the solid angle presented by the detector between the angles  $\theta$  and  $\theta + d\theta$ , can be written as

$$\sin \theta \, d\theta \, \Delta \phi \quad (35)$$

where  $\Delta \phi \approx \tan \Delta \phi \approx \frac{l}{h}$  (36)

the meaning of the symbol h being explained in the figure. Because of the presence of the collimator, the angle  $\theta$  was not a continuous variable. Thus, in the case shown in the figure, there are two allowed angular intervals, in which the particle could travel, viz  $\Delta \theta_1$  around a mean value of  $\theta_1$ , and  $\Delta \theta_2$  around a mean value of  $\theta_2$ . The total solid angle presented by the detector at the point P was, therefore,

$$d\Omega = \Delta \phi (\sin \theta_1 \Delta \theta_1 + \sin \theta_2 \Delta \theta_2) \quad (37)$$

$\Delta \theta$  was in general very small, of the order of one or two degrees, so that the value of  $\sin \theta$  remained essentially constant over the range and using the average value of  $\theta$  in the sine, was justified.

The expression within brackets on the right hand side of eqn. (37) was estimated by actual measurements on the scale drawing of the target, for various points P distributed along the axis.  $\Delta \phi \sum \sin \theta \Delta \theta$

was then plotted against t, the distance of the point P from any arbitrary referent point on the axis AB.

(Usually this was chosen as the extreme limit, from which a detectable event could arise, i.e., for which  $d\theta \rightarrow 0$ ). The area under the graph gave

$$\Delta\phi \int \sin\theta d\theta dt = t. \Delta\Omega$$

The cross-section in centre-of-mass was calculated from the laboratory cross-section given by eqn. (31) with the help of the formula

$$\left(\frac{d\sigma}{d\Omega}\right)_{c.m.} = \left(\frac{d\sigma}{d\Omega}\right)_{lab} \times \frac{d\Omega}{d\Omega^*} \quad (38)$$

where

$$\frac{d\Omega}{d\Omega^*} = \frac{\sin\theta d\theta d\phi}{\sin\theta^* d\theta^* d\phi} = \frac{d(\cos\theta)}{d(\cos\theta^*)} \quad (39)$$

the asterisk referring to the centre-of-mass system. It can be shown that  $\theta$  and  $\theta^*$  are connected by the relationship

$$\tan\theta = \sqrt{1-\beta^2} \frac{\sin\theta^*}{\gamma + \cos\theta^*} \quad (40)$$

so that the above ratio is reducible to the form

$$\frac{d\Omega}{d\Omega^*} = \frac{\gamma \cos\theta^* + 1}{(\gamma^2 + 2\gamma \cos\theta^* + 1)^{3/2}} \quad \{\beta^2 \ll 1\} \quad (41)$$

where

$$\gamma = \frac{\beta m_{He^4}}{b} \quad (42)$$

$\beta$  = velocity of the centre-of-mass in units of light velocity =  $\frac{E_\gamma}{E_\gamma + m_{He^4}}$  (43)

$h_e$  = momentum in centre-of-mass

$$= \frac{1}{2N} \sqrt{\left\{ N^2 - (m_{He^4} + m_{\pi^0})^2 \right\} \left\{ N^2 - (m_{He^4} - m_{\pi^0})^2 \right\}} \quad (44)$$

N being = energy in centre-of-mass

$$= (E_\gamma + m_{He^4}) \left( 1 - \frac{\beta^2}{2} \right) \quad (45)$$

mass, and momentum being measured in energy units 53).

Chapter IV - RESULTS.

Section (A) - The Photomeson Production Cross-sections.

(i)  $\theta = 20^\circ$ .

At this angle the recoil energies were the largest and so it was possible to investigate the most extensive range of the energy spectrum, and consequently, of the excitation function as well. The experimental data were acquired in two runs, each extending over a period of four days (about 10 hours of overall running time/day). The details are presented below

(a) High Energy Run

Target pressure = 65 lbs/square inch  $\approx 4 \frac{1}{3}$  atmospheres

Chamber pressure = 3 atmospheres of Argon and Methane.

$E_2 \text{ max} = 23 \text{ MeV}$  which was

$\equiv 28.5 \text{ MeV}$  when the  $\alpha$ -particle was just entering the chamber

$\equiv 33 \text{ MeV}$  at creation, after allowing for the mean energy loss within the target.

$E_2 \text{ min} = 2.6 \text{ MeV}$  which

$\equiv 22.2 \text{ MeV}$  at creation.

This corresponds to the range  $256 < E_\gamma < 306 \text{ MeV}$ .

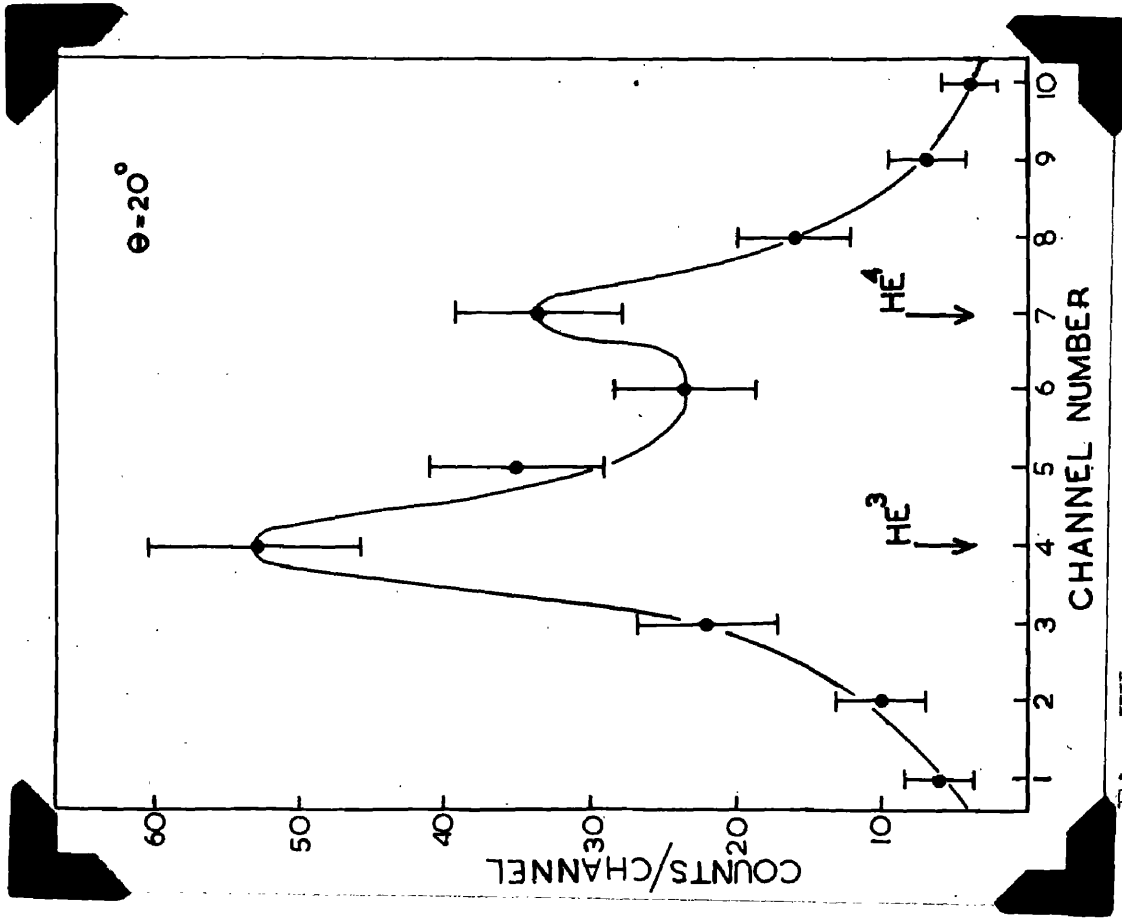


Fig. XX.

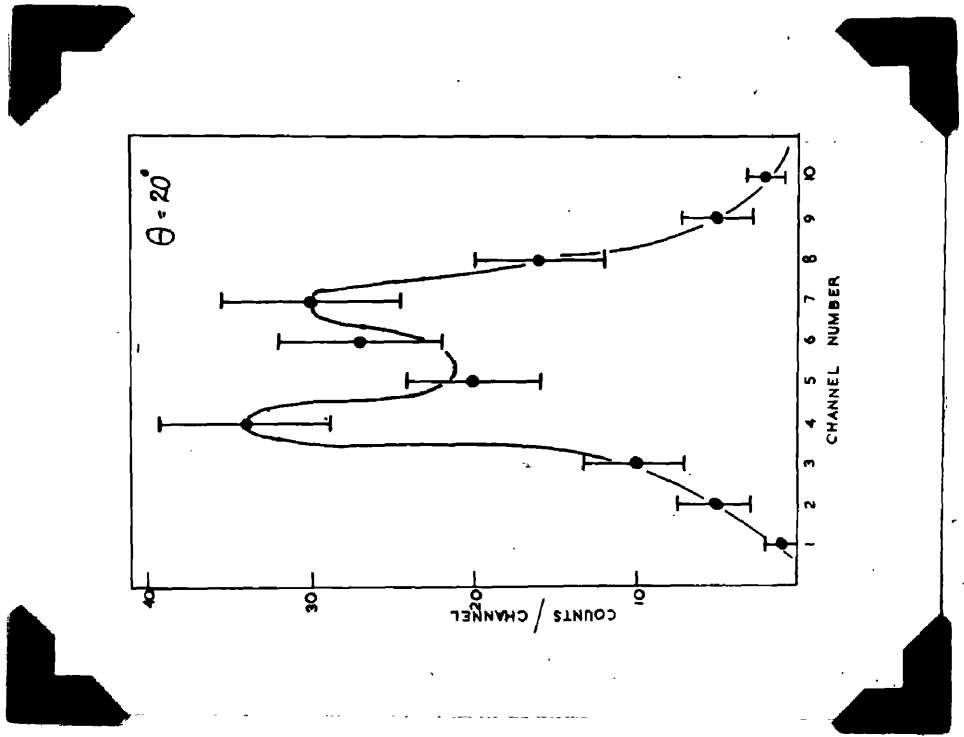


Fig. XXI

Histograms from the high- and low-energy runs at  $20^\circ$

respectively.

These extreme limits were calculated from the observed position of the spots on the screen, and included most of the events actually recorded. The few that lay outside this range were ignored, for the analysis had to be restricted to the region, where the detector and the display unit could be expected to operate reliably.

The mass spectrum is shown in Fig. XX. To estimate the number of  $\text{He}^4$ 's from it, one could simply take the sum of the number of counts in channels 6-10, to a close degree of approximation. The error introduced, because of the two peaks not being exactly <sup>of</sup> the same height was a second order effect, since the contribution of each peak three channels away, on either side of the central channel was itself quite small. In fact, the value of the total number deduced in this way agreed remarkably well with that arrived at, by a more refined method of analysis; such as drawing a curve to give the best fit through the points, reflecting the two edges about the central lines through the peaks, and then computing the areas under the two curves. In any case, the standard statistical deviations were large in comparison to the uncertainty in estimating the relative number of  $\text{He}^3$ 's and  $\text{He}^4$ 's,

so that the latter only made a relatively small additional contribution to the overall uncertainty in the cross-section. All uncertainties shown in the graphs or in the tables include only these two effects, though the contribution from the latter had to be estimated rather arbitrarily. In addition to these, there will, of course, be an additional uncertainty in the absolute cross-section scale, due to errors in beam intensity calibration (claimed to be accurate to within 10%), pressure measurement in the target, and so on.

To obtain an excitation function, the total  $E_\gamma$  spread of 50 MeV was divided into two equal parts, and the numbers of recoil  $\text{He}^4$ 's in the two ranges, estimated separately, by the method of the last paragraph. A line was drawn in the appropriate place, at right angles to the curves in Fig. XIV (page 55) and the analysis done separately for the two halves.

The plot of  $\sum \text{Sin } \theta \Delta \theta$  against "t" is shown in Fig. XXII.

(b) Low energy run

Target pressure =  $2\frac{1}{2}$  atmospheres

Chamber pressure =  $1\frac{1}{2}$  atmospheres.

The mass spectrum is shown in Fig. XXI.

Fig. XXII The  $t \cdot \Delta\Omega$  plot.

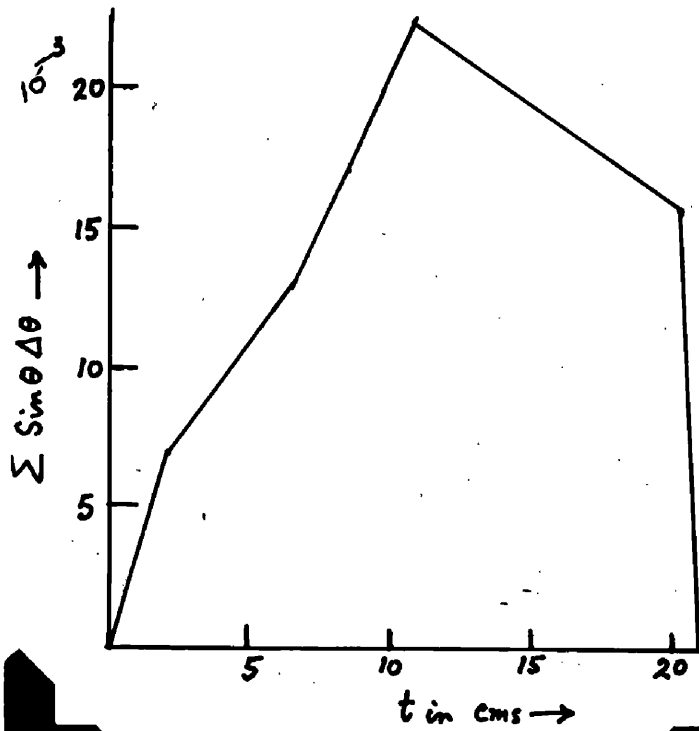


Fig. XXIII. Excitation function for the reaction  $\gamma + He^4 \rightarrow \pi^0 + He^4$

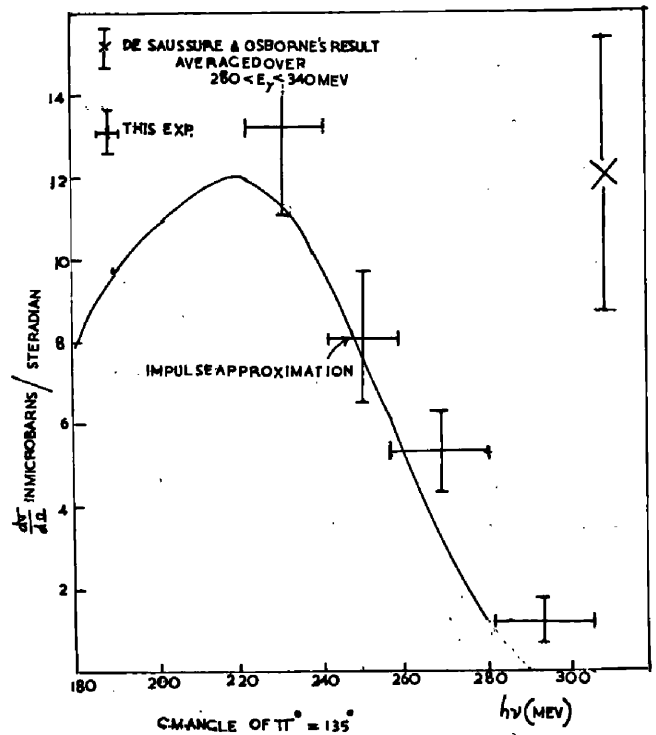


Table IV Results of the 20° Run.

Nature of Run	$\Delta E_\gamma$ at creation	$\Delta E_\gamma$	Total "Q"	$N_\gamma$	n	N	t, $\Delta t$	$\frac{d\Omega'}{d\Omega}$	$\left(\frac{d\sigma}{d\Omega}\right)$ c.m.
High Energy	27.5 to 33 Mev.	281 - 306 Mev.	22.4 x 10"	15.2 x 10 <sup>10</sup>	1.13 x 10 <sup>20</sup>	13 ± 5	.14 cm -strahlung	0.22	1.25 ± .5 $\mu\text{b}/\text{sterad}$
	22.5 to 27.5 Mev.	256 - 381 Mev.	22.4 x 10"	18.4 x 10 <sup>10</sup>	1.13 x 10 <sup>20</sup>	71 ± 9	.14 cm -strahlung	0.22	5.4 ± .7 "
Low Energy	19.4 to 23 Mev	241 - 260 Mev.	13.6 x 10"	9.13 x 10 <sup>19</sup>	6.46 x 10 <sup>19</sup>	30 ± 6	.14 cm -strahlung	0.22	8.0 ± 1.6 "
	16 to 19.4 Mev	223 to 241 Mev	13.6 x 10"	9.3 x 10 <sup>10</sup>	6.46 x 10 <sup>19</sup>	50 ± 8	.14 cm -strahlung	0.22	13.2 ± 2.1 "

The total energy spectrum was again divided into two parts. The combined data for the high and low energy runs are shown in Table IV.

Fig. XXIII shows the excitation function. The solid curve is based on the impulse approximation, and actually refers to a laboratory angle of  $135^\circ$  for the meson, which corresponds to a value of slightly  $> 135^\circ$  in the centre-of-mass. However, the ratio  $\frac{d(\text{Cos } \theta)}{d(\text{Cos } \theta^*)}$  for  $\pi^0$  is very nearly equal to unity (because the pion velocity in centre-of-mass is large, compared to the velocity of the centre-of-mass itself, unlike that of the recoiling  $\text{He}^4$  particle, which is much more massive). The experimental points, on the other hand refer to  $45^\circ$  centre-of-mass angle for the  $\text{He}^4$ , i.e.  $135^\circ$  in centre-of-mass for the  $\pi^0$ . The cross at the top right hand corner is De Saussure and Osborne's result, averaged over a photon energy range 280 - 340 MeV.

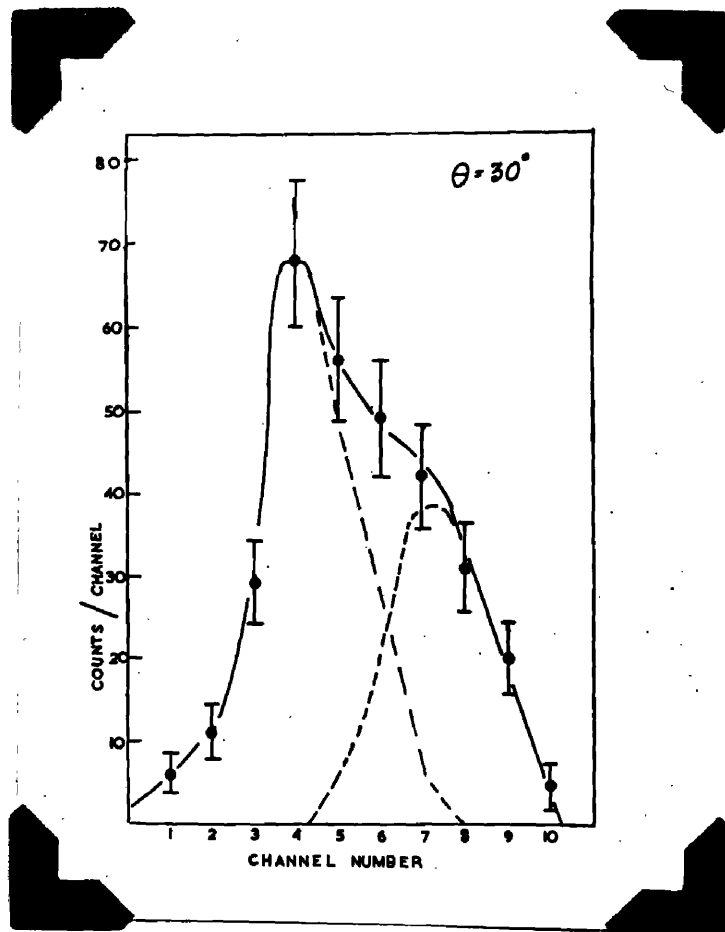


Fig. XXIV. The mass spectrum at  $\theta = 30^\circ$ .

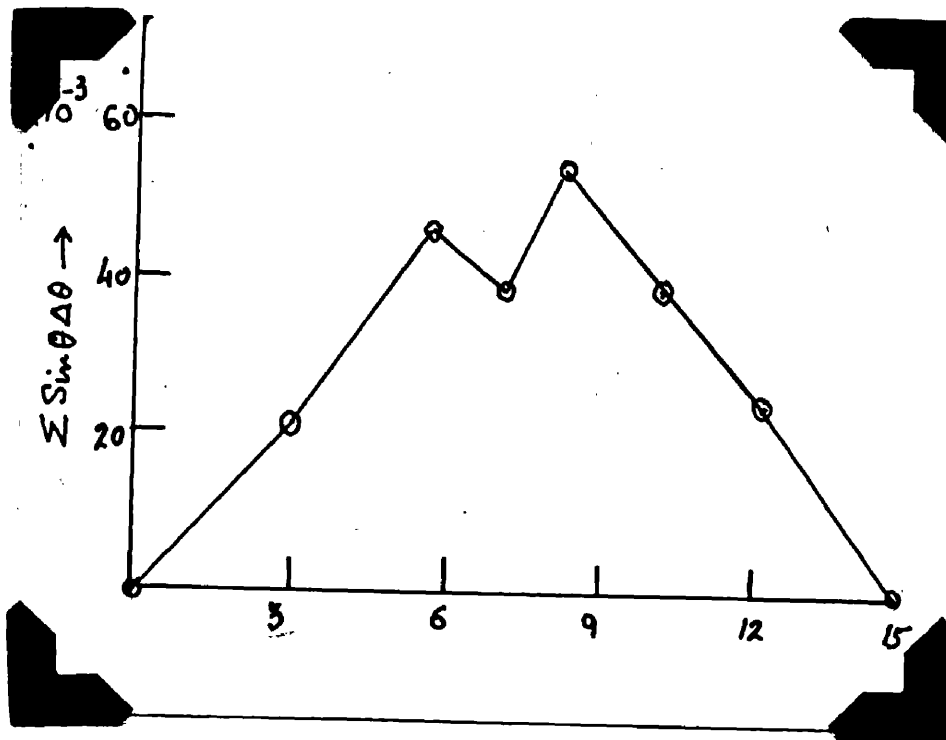


Fig. XXV. The  $t, \Delta\Omega$  plot.

Table V Results of the 30° run.

$\Delta E_\alpha$	$\Delta E_\gamma$	Q	N $\gamma$	$\theta^*$	N	n	$\frac{d\Omega'}{d\Omega}$	$\left(\frac{d\sigma}{d\Omega}\right)$ c.m.
18-29 MeV.	254-313 MeV.	27.3 x 10"	4.8 x 10"	65°	125 ± 30	9 x 10 <sup>19</sup>	0.25	4.0 ± .9 $\mu\text{bn}/\text{steradian}$

(ii)  $\theta = 30^\circ$

Target pressure = 53 lbs/sq. inch  $\approx 3\frac{1}{2}$  atmospheres

Chamber pressure =  $2\frac{1}{2}$  atmospheres

The resolution at this angle was unfortunately rather poor, in fact the worst in the whole experiment. As Fig. XXIV shows, the peaks of He<sup>3</sup>'s and He<sup>4</sup>'s were not at all separated. This could well have been due to a high electron background, caused by the  $\gamma$ -ray beam hitting the inside walls of the target pipe or the lead collimator in front of the pipe. This would cause most of the pulses to sit on a pile-up "pedestal", and would then tend to make each individual peak rather lop-sided, with a tail on the high pulse height side. The observed distribution has been analysed into two individual peaks on this assumption. As the resolution was so poor, it was not considered worthwhile to attempt a detailed analysis to find out an excitation function as at  $\theta = 20^\circ$ , but only an average differential cross-section was calculated. Fig. XXV shows the  $t \cdot \Delta\Omega$  plot.

Table V gives the values of the various parameters.

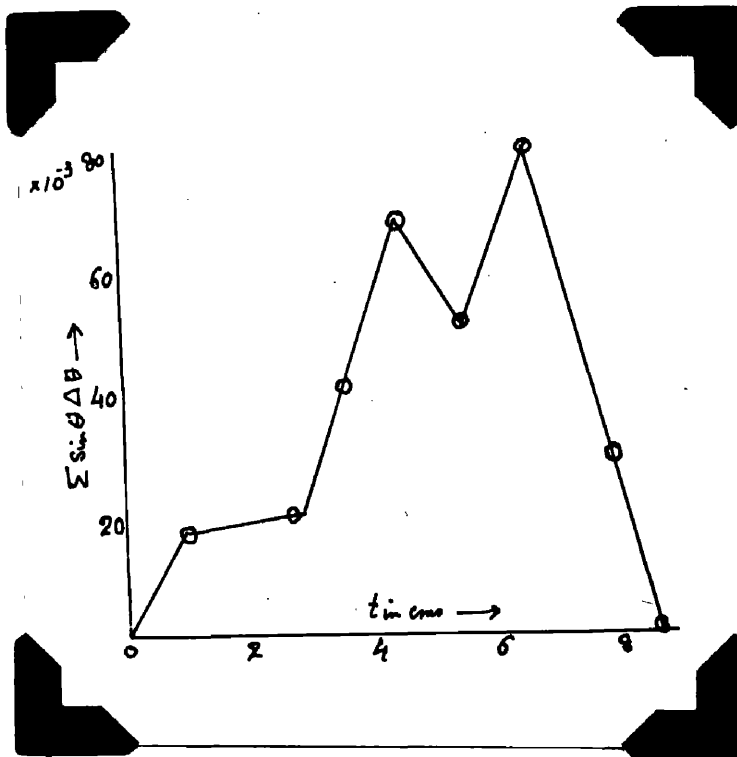


Fig. XXVI. The  $t. \Delta \Omega$  plot.

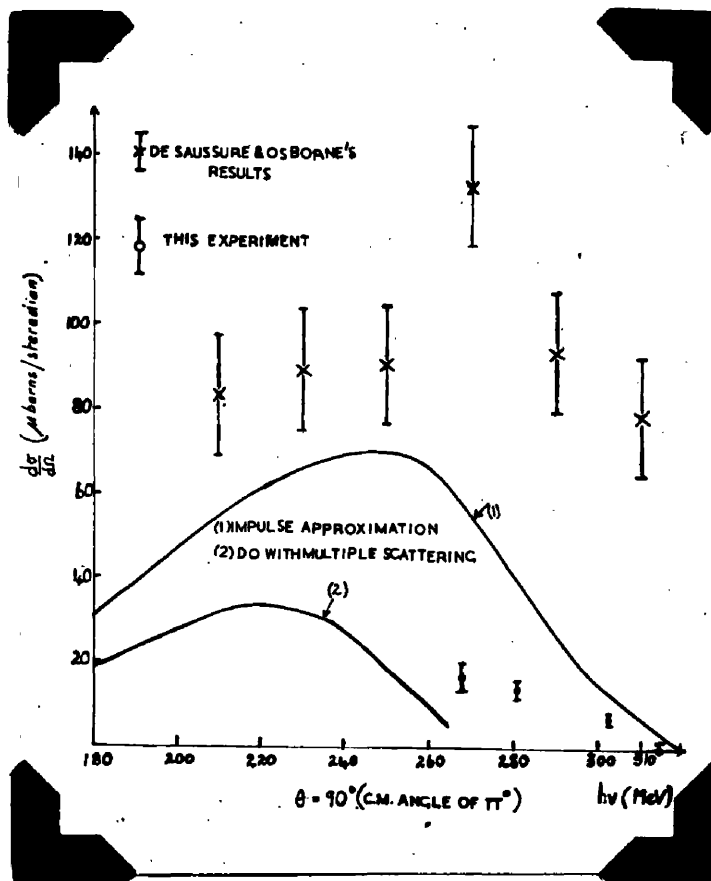


Fig. XXVII. The excitation function at  $\sim 90^\circ$  c.m. angle for the  $\pi^\circ$ .

(iii)  $\theta = 40^\circ$

Target pressure =  $2\frac{1}{2}$  atmospheres

Chamber pressure =  $1\frac{1}{2}$  atmospheres

The whole data were acquired in one series of runs, under the same pressure conditions, but were subdivided into 3 groups for the purpose of evaluating an excitation function. The results are shown in Table VI. Fig. XXVI is the  $t \cdot \Delta\Omega$  plot. The histogram is shown in Fig. XVIII, page 61.

It must be remembered, that it was rather difficult to estimate  $\Delta E_\alpha$  at creation precisely, from the observed range of  $E_2$ 's, when its absolute value was so small as in range 3. The above only represents a mean value with a possibility of a wide scatter because of the different paths followed by the particle in travelling from the target to the detector. Nevertheless, the results should still be of interest in showing the general trend of the excitation function. Another factor of interest was that  $t \cdot \Delta\Omega$  hardly changed from one angle to another. For, as the chamber approached the target more and more closely with increasing  $\theta$ ,  $\Delta\Omega$  increased, but the value of "t" went down. Similarly an increase in cross-section at larger angles was offset by the fact that lower pressures had to be used to reduce self-absorption

Table VI Results of the 40° run.

Range No.	$\Delta E_\alpha$ at creation in MeV.	$\Delta E_\gamma$ in MeV.	Q	$N_\gamma$	n	N	$\frac{d\Omega'}{d\Omega}$	t. $\Delta\Omega$	$\left(\frac{d\sigma}{d\Omega}\right)$ cm.
1	18-22.3	291-315	$18.4 \times 10^{10}$	$39 \pm 7$					$7.2 \pm 1.4$ $\mu\text{bn}/\text{strand}$
2	15.3 to 18	272-291	$2.94 \times 10^{12}$	$17.5 \times 10^{10}$	$6.4 \times 10^{19}$	$75 \pm 10$	0.282	0.13 cm-strand	$14.4 \pm 1.8$ "
3	14.4 50 15.4	263-272	$8.7 \times 10^{10}$			45			$17.1 \pm 3.7$ "

(because of lower recoil energies), and thus the counting rate stayed pretty well constant, at the miserably low value of  $\sim 10$  counts/hour (with the normally available beam intensity of  $\sim 10^9$  equivalent quanta/minute).

Fig. XXVII shows the experimental cross-sections, together with theoretically calculated values of the excitation function (at a laboratory angle of  $90^\circ$  for the  $\pi^0$ ). The top curve is based on pure and simple impulse approximation, the lower one includes the multiple scattering correction as well. The crosses are the experimental results of De Saussure and Osborne.

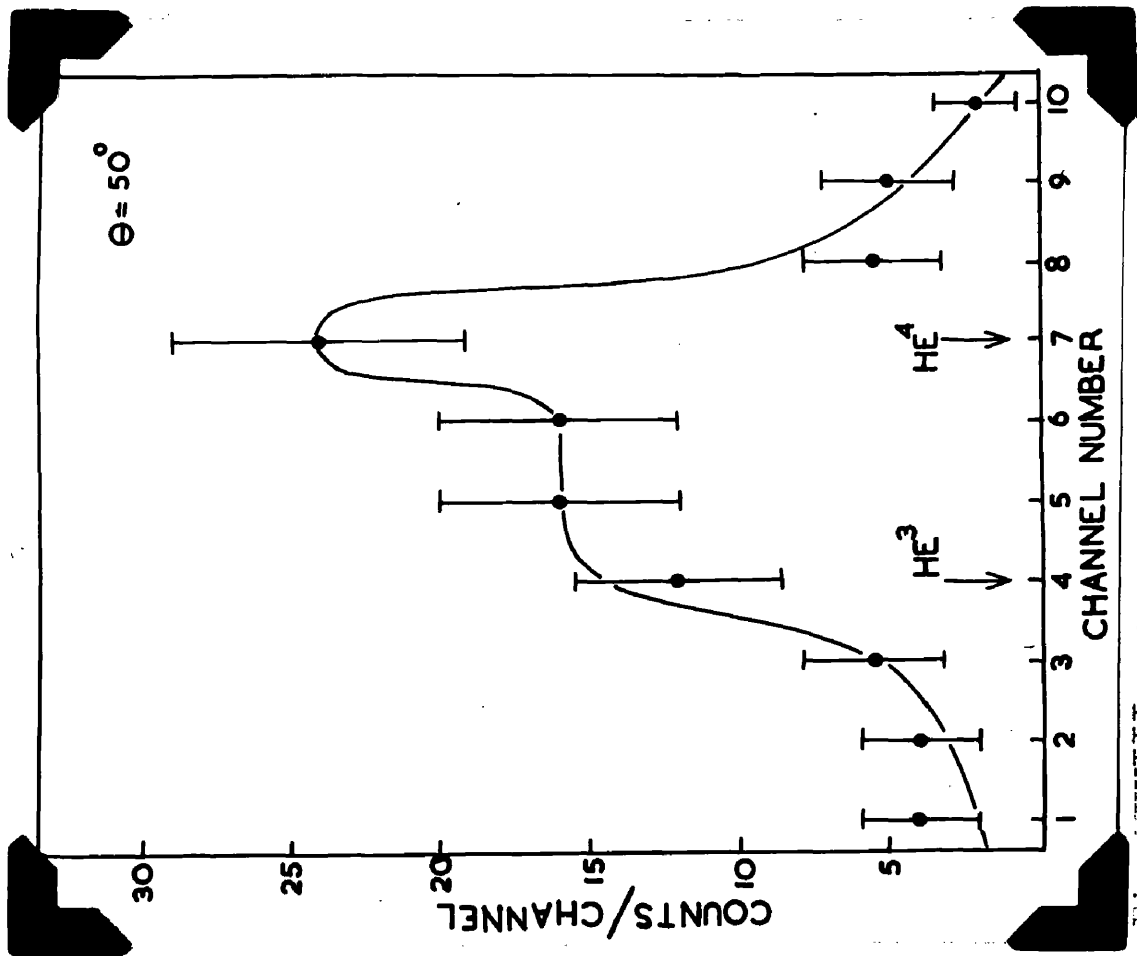


Fig. XXVIII. The mass spectrum at  $\theta = 50^\circ$ .

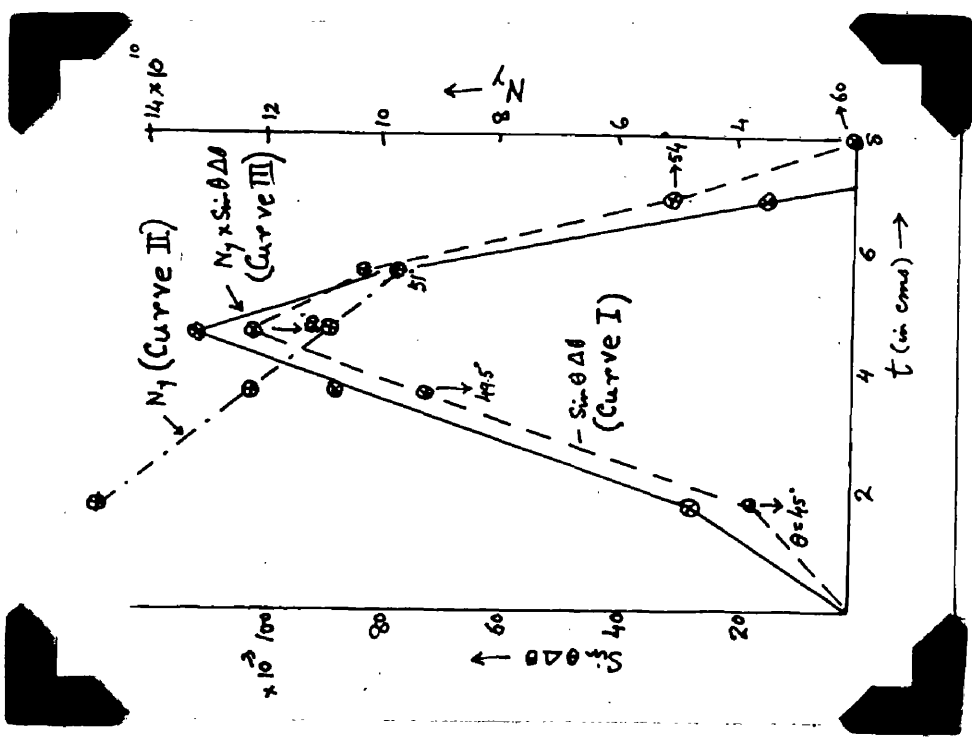


Fig. XXIX. The evaluation of

$t \cdot \Delta \Omega \cdot N_\gamma$  at  $\theta = 50^\circ$ .

(iv)  $\theta = 50^\circ$

Target pressure = 2.1 atmospheres

Chamber pressure = 1 atmosphere

Fig. XXVII shows the mass spectrum. The statistics are rather poor because of low available beam intensity. Owing to machine trouble, only about a third of the total Q used at other angles was available in this case, over a running time of four days.

The laboratory angles at which recoil nuclei were accepted varied roughly over the range  $45^\circ - 55^\circ$ . As a reference to the reaction dynamics diagram in Fig. VI, page 24, will show, for a given value of  $\Delta E_\alpha$  at creation, there is a wide variation in  $\Delta E_\gamma$  and hence in  $N_\gamma$  with angle, in this region. Therefore, the effective value of  $t \cdot \Delta \Omega \cdot N_\gamma$  had to be computed by graphical integration. Fig. XXIX shows how this was done. Curve I, is the usual plot of  $\sum \sin \theta \Delta \theta$  against  $t$ . Curve II, represents  $N_\gamma$  at each different value of  $\theta$ , calculated from Fig. VI. Curve III was obtained by multiplying the corresponding ordinates of I, and II. The area under this gave  $t \cdot \Delta \Omega \cdot N_\gamma$ . It might be pointed out that in this particular angle,  $\sum \sin \theta \Delta \theta$  was just  $= \sin \theta, \Delta \theta$ , since only one

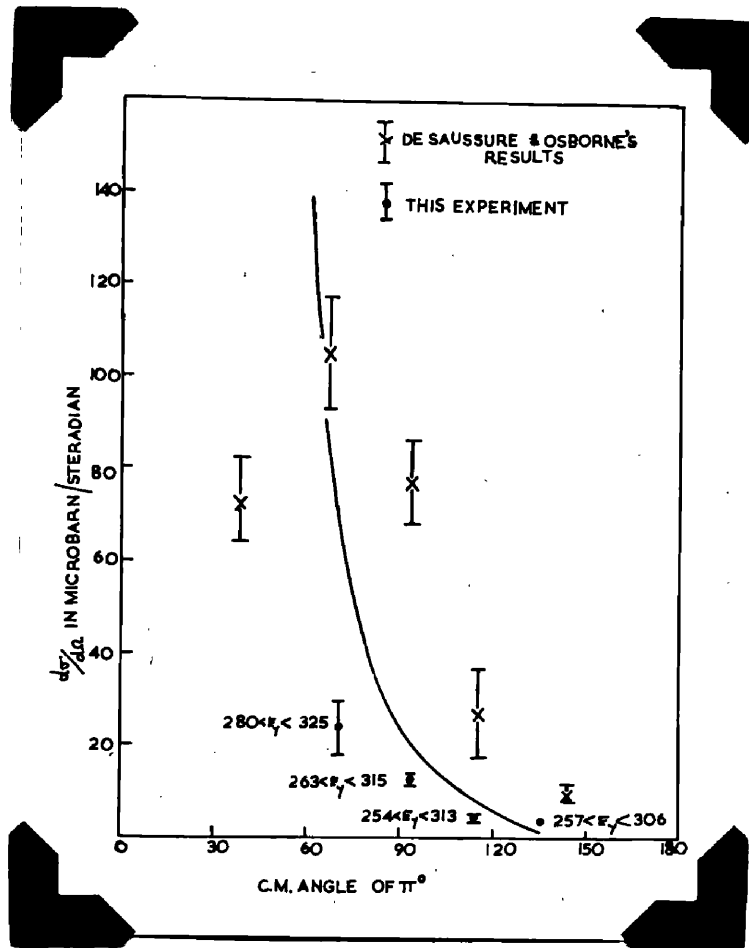


Fig. XXX. The angular distribution for the reaction  $\gamma \rightarrow He^4 \rightarrow \pi^0 + He^4$ . De Saussure & Osborne's results are averaged over the range  $280 < E_\gamma < 340$  Mev. The solid curve is based upon the impulse approximation & refers to a mean  $E_\gamma = 290$  Mev. The energy ranges over which the results of this experiment are averaged at different angles are indicated on the figure.

Table VII Results of the 50° run.

$\Delta E_\alpha$ at creation	$\Delta E_\gamma$	Q	t.A.Q. $N_\gamma$	N	n	$\frac{d\Omega'}{d\Omega}$	$\left(\frac{d\sigma}{d\Omega}\right)_{cm.}$
10.5 to 16 Mev.	280-325 Mev.	1.1 x 10 <sup>12</sup>	1.43 x 10 <sup>10</sup> cm - <i>Stadian</i>	58	5.5 x 10 <sup>19</sup>	0.33	24.3 ± 5.3 <i>µbn/strand</i>

continuous angular interval was allowed for any point on the axis of the target. This somewhat simplified the calculation. Table VII shows the result.

Fig. XXX represents the angular distribution. The  $E_\gamma$  spread over which the cross-section is averaged at each angle is indicated on the diagram. The curve is based on impulse approximation. The crosses are De Saussure and Osborne's results averaged over  $280 < E_\gamma < 340$  MeV range. As usual, the experimental points refer to centre-of-mass angles of the pion, whereas the theoretical curve is based on laboratory angles. The difference, however, is small.

Section (B) - The  $\text{He}^3$  Cross-sections.

If all the  $\text{He}^3$ 's obtained in this experiment are assumed to come from the two-body photodisintegration process  $\gamma + \text{He}^4 \longrightarrow \text{He}^3 + n$ , as was done by De Saussure and Osborne, then the cross-sections in the laboratory system are as follows:-

$$69 < E_\gamma < 90 \text{ MeV. } \left( \frac{d\sigma}{d\Omega} \right)_{\theta = 20^\circ} = 19.3 \pm 2.4 \text{ } \mu\text{bn/sterad}$$

$$87 < E_\gamma < 117 \text{ MeV. } \left( \frac{d\sigma}{d\Omega} \right)_{\theta = 20^\circ} = 11.7 \pm 1.2 \text{ } "$$

$$78 < E_\gamma < 113 \text{ MeV. } \left( \frac{d\sigma}{d\Omega} \right)_{\theta = 30^\circ} = 10.4 \pm 1.7 \text{ } "$$

$$67 < E_\gamma < 96 \text{ MeV. } \left( \frac{d\sigma}{d\Omega} \right)_{\theta = 40^\circ} = 11.8 \pm 1.2 \text{ } "$$

$$62 < E_\gamma < 84 \text{ MeV. } \left( \frac{d\sigma}{d\Omega} \right)_{\theta = 50^\circ} = 12.8 \pm 4 \text{ } "$$

$$90 < E_\gamma < 138 \text{ MeV. } \left( \frac{d\sigma}{d\Omega} \right)_{\theta = 90^\circ} = 9.6 \pm 2 \text{ } "$$

Chapter V - INTERPRETATION AND DISCUSSION.

At the present state of knowledge, the results of this experiment have to be interpreted in terms of the impulse approximation. This, as has been already pointed out in Section B, Chapter I, treats photomeson production at a complex nucleus as essentially a single nucleon process. If  $T$  be the transition operator for photoproduction of mesons at Helium, and  $T_i$  the corresponding operator for the  $i$ th free nucleon, then on the impulse approximation,

$$T = T_1 + T_2 + T_3 + T_4 \quad (46)$$

The matrix element of  $T$  must be taken and averaged over the initial and final momentum distributions of the nucleons inside the nucleus, for although these nucleons are treated as free during the interaction, they retain the momentum distribution imposed upon them by the nuclear binding potential. Therefore, the transition probability amplitude for the production of a meson of momentum  $\underline{q}$ , by a photon of momentum  $\underline{\nu}$  (momentum and energy all measured in natural units with  $\hbar = c = 1$ ) can be expressed as

$$\langle \underline{q} | T | \underline{\nu} \rangle = \sum_{j=1}^4 \int d\underline{r}_1 d\underline{r}_2 d\underline{r}_3 d\underline{r}_4 \Psi^*(1,2;3,4) e^{-i\underline{p} \cdot \underline{R}} (\underline{q} | T_j | \underline{\nu}) \times e^{i(\underline{\nu} - \underline{q}) \cdot \underline{r}_j} \Psi(1,2;3,4) \quad (47)$$

where  $\Psi(1,2,3,4)$  is the normalised ground state wavefunction of the  $\alpha$ -particle depending on both the space and spin co-ordinates of the nucleons and is antisymmetric under the interchange of (1 and 2) and of (3 and 4) in compliance with the Pauli Principle.

$$\underline{R} = \frac{1}{4} (\underline{r}_1 + \underline{r}_2 + \underline{r}_3 + \underline{r}_4) \quad (48)$$

is the co-ordinate of the centre-of-mass of the  $\alpha$  particle,  $\underline{r}_j$  being the co-ordinate of the  $j^{\text{th}}$  nucleon.

$\underline{p}$  is the recoil momentum of the nucleus after photo-production. Assuming that

$$\underline{q} | T_j | \underline{v} = \underline{\sigma}(j) \cdot \underline{k}_0 + L_0 \quad (49)$$

(which necessarily implies that the dependence of the matrix element on the actual momenta of the struck nucleon inside the nucleus before and after collision is neglected) eqn. (47) can be expressed in the form

$$\langle \underline{q} | T | \underline{v} \rangle = 4L_0 \int d\underline{r}_1 d\underline{r}_2 d\underline{r}_3 d\underline{r}_4 \Psi^*(\underline{r}_1, \underline{r}_2, \underline{r}_3, \underline{r}_4) e^{-i\underline{p} \cdot \underline{R}} \times e^{i(\underline{v}-\underline{q}) \cdot \underline{r}_j} \Psi(\underline{r}_1, \underline{r}_2, \underline{r}_3, \underline{r}_4) \quad (50)$$

It is seen that the spin flip part  $\underline{k}_0$  of the matrix element for photoproduction at a single nucleon does not enter in eqn. (50) and, therefore, does not contribute to the photoproduction process from helium. This is because

the spin of the helium nucleus is zero both in the initial and final stages. Spin flip of one of the constituent nucleons, therefore, leads to a disintegration of the nucleus, and the process is no longer elastic.

On integrating over various possible values of the recoil momenta for the  $\alpha$ -particle, one finally obtains

$$\begin{aligned} \left(\frac{d\sigma}{d\Omega}\right)_q &= \frac{1}{(2\pi)^2} \frac{q_0^2}{1 + \frac{q_0}{4Mq} (q - v \cos\theta)} \times 16 |L_0|^2 |F(p)|^2 \\ &= A(q_0, \theta) \times 16 |L_0|^2 |F(p)|^2 \end{aligned} \quad (51)$$

where  $v = q_0 + \frac{|\underline{v} - \underline{v}|^2}{8M}$

$v$  and  $q_0$  being the energies of the photon and the meson respectively, and  $M$  is the nucleon mass.

$$F(p) = \int ds_2 ds_3 ds_4 \left| \psi(s_2, s_3, s_4) \right|^2 e^{-ip \cdot (s_2 + s_3 + s_4)/4} \quad (52)$$

is the form factor of the Helium nucleus, exactly analogous to the corresponding expression for the

deuteron, defined by eqn. (7), page 11 . Chapter I,

$\underline{S}_j$  in the above expression is the relative co-ordinate of the  $j^{\text{th}}$  nucleon with respect to any one of the rest as origin.

Thus according to eqn. (51) in order to be able to derive the value of the differential cross-section for elastic  $\pi^0$  production process from helium, from the experimentally measured cross-sections from hydrogen, one has not only to use the reaction kinematics to deduce the value of the function  $A(q_0, \theta)$ , but

(i) should also have a theory giving the relative contributions of the spin flip and non-spin flip parts to the matrix element for photoproduction at a single nucleon, since this cannot be determined from experimental data alone;

(ii) and must also postulate a model for the helium nucleus to evaluate the form factor.

The value of  $|L_0|^2$  used in the calculation of Stoodley's theoretical curves (private communication) has been obtained from Chew's <sup>54)</sup> cut-off theory, in which

$$\left(\frac{d\sigma}{d\Omega}\right)_{\text{c.m.}}^{\text{for proton}} = B \left[ |m_1 - e_2|^2 \cos^2 \theta + \left\{ \frac{1}{2} |m_1 + e_2|^2 + 2|m_1|^2 \right\} \sin^2 \theta \right] \quad (53)$$

where  $\theta$  is the c.m. angle of the  $\pi^0$ ,  $|m_1|$  and  $|e_2|$  are the effective matrix elements for transition to the  $3/2, 3/2$  state due to magnetic dipole and electric quadrupole radiations respectively, and B does not involve the angle  $\theta$ . If this, the spin-independent term is

$$|L_0|^2 = 2B |m_1|^2 \sin^2 \theta = 16 \pi^2 a_{m_1}^2 \frac{\nu_c}{q_{0c}^2 q_c^4} \sin^2 \delta_{33} \sin^2 \theta \quad (54)$$

The  $\sin^2 \theta$  dependence can, of course, be predicted from purely phenomenological considerations based on angular momentum and parity conservation, assuming a purely magnetic dipole absorption of the incident  $\gamma$ -ray. The latest measurements on the angular distribution of  $\pi^0$ 's from hydrogen<sup>16,14)</sup> ( $2 + 3 \sin^2 \theta$ ), certainly supports this assumption.  $\delta_{33}$

is the meson-nucleon scattering phase shift in the  $3/2, 3/2$  state, as only the particular isotopic spin state  $T = 3/2$  has been taken into consideration. This has been partially justified on page 8. The subscript C in formula (54) refers to the centre-of-mass system, and  $a$  and  $m_1$  are real energy independent constants whose values were adjusted to give the best fit to the Cal. Tech. measurements of the excitation function at  $90^\circ$ . In evaluating  $a_1$  and  $m_1$ ,  $|e_2|$  in formula (53)

was assumed to be = 0.

As regards calculation of the form factor, two different types of nuclear wave function have been used. The curves with which the experimental results are actually compared, are based on a Gaussian wave function of the form

$$\Psi (r_1, r_2, r_3, r_4) = N_G^{1/2} \exp. (-\mu_{\alpha G}^2 \sum |r_{ij}|^2) \quad (55)$$

where  $r_{ij} = r_j - r_i$  is the relative co-ordinate of the nucleons  $i$  and  $j$

$N_G^{1/2}$  is a normalising factor

$\mu_{\alpha G}$  is a parameter which was adjusted to give the best fit to the binding energy and radius of the  $\alpha$ -particle. Eqn. (55), of course, gives the radial wave function assuming the ground state to be a pure singlet  $^1S_0$  configuration (over 97% according to Irving<sup>55</sup>). Using Hofstadter<sup>56</sup>) et. al's value for the r.m.s. radius of the  $\alpha$ -particle  $R = 1.4 \times 10^{-13}$  cm, and the known 28 MeV binding energy,

$$\frac{1}{\mu_{\alpha G}} \text{ has been chosen } = 3.3 \times 10^{-13} \text{ cm} \quad (56)$$

The validity of the Gaussian wave function in case of a light nucleus like Helium is doubtful. Its chief defect is the bad asymptotic behaviour since it falls off too rapidly with increasing separation between the nucleons. This implies a rather diffuse momentum distribution of the nucleons inside the nucleus, which though verified by the experimental results of high energy proton scattering in case of Carbon and Oxygen <sup>57)</sup> is in sharp disagreement with the results from deuterium. Therefore, Irving <sup>58)</sup> has examined wave function of the following type for the  $\alpha$ -particle

$$\psi(r_1, r_2, r_3, r_4) = N_I^{1/2} \frac{\exp. \left\{ -\mu_{\alpha I} (\sum r_{ij}^2)^{1/2} \right\}}{(\sum r_{ij}^2)^{1/2}} \quad (57)$$

which is similar to the Hulthen wave function for the deuteron. Calculations using an Irving type wave function with  $\frac{1}{\mu_{\alpha I}} = 1.7 \times 10^{-13} \text{cm}$  gave values of the differential cross-section for elastic production on Helium which were 30% lower than those given by the actual curves in Figs. XXIII, XXVIII and XXX, at all angles and energies.

Using eqn. (55), the form factor reduces to the simple form

$$|F(p)|^2 = \exp. \left\{ -\frac{3p^2}{64\mu_{\alpha G}^2} \right\} \quad (58)$$

The role of the form factor in modifying the cross-section is thus seen to be very important. Because of the exponential  $(-p^2)$  dependence, it falls off extremely rapidly with increasing  $p$ . Thus it tends to reduce the cross-section whenever there is a large momentum transfer to the recoiling nucleus, i.e. at forward angles, and at high energies. Physically, therefore, the form factor may be interpreted as a probability that the  $\alpha$ -particle will stick together as one unit, as it must if the process is to be elastic, when it is given a recoil momentum  $p$ . Therefore, eqn. (51) gives an angular distribution for the process  $\gamma + \text{He}^4 \rightarrow \pi' + \text{He}^4$  which, as is clear from Fig. XXX, page 78, is strongly peaked in the forward angles of emission of the meson (remembering that  $|L_0|^2 \propto \sin^2\theta$ ). Also, the excitation function drops off rapidly beyond  $E_\gamma \sim 250$  MeV (though the single nucleon cross-section shows a maximum round about 320 MeV). Thus at  $90^\circ$ ,  $|F(p)|^2$  decreases monotonically from .6 to .13 for  $E_\gamma$  varying between 180 to 320 MeV.

As Fig. XXIII, page 73, shows, the experimental results are in good agreement with this simple theory at this particular angle. At  $\phi = 90^\circ$ , however, the experimental points lie in between the pure impulse

approximation calculation, and one with multiple scattering correction. The latter was based essentially on an extension of the Chapplear 33) Brueckner formalism for the corresponding case with the deuteron. It assumed a regular tetrahedron model for the helium nucleus, and included only on the "energy-shell" scattering from the  $3/2, 3/2$  state. It also ignored the possibility of  $\pi^0$  production from helium proceeding via charged meson production from one nucleon, followed by subsequent charge exchange scattering from another nucleon. Thus while the general trend of a reduction in cross-section is likely to be valid, the exact amount of reduction as calculated, is of doubtful accuracy. The calculation has not been carried out at other angles.

The measured cross-sections are in gross disagreement with the results of De Saussure and Osborne. At forward angles of emission of the meson, the form factor is close to unity ( $\beta \approx 0$ ), and the cross-section is given by the impulse approximation independent of the helium radius, or the type of wave function chosen. So the validity of the impulse approximation hypothesis could best be tested in this region. Unfortunately, this was the most difficult region to investigate, for the experiment relied on a measurement of  $\beta$  in two fragments.

However, the experimental angular distribution can be

extrapolated to zero angle on the assumption of an explicit form for the form factor.

De Saussure and Osborne's results do indeed extrapolate to a reasonable zero angle value. The value of the r.m.s. radius for the  $\alpha$ -particle which they derive from their measured angular distribution is, however,  $.93 \times 10^{-13}$  cm (Fig. 7, of their paper). If one takes the more accurate and reliable Hofstadter value of  $1.43 \times 10^{-13}$  cm, the cross-section at  $90^\circ$  in centre-of-mass assuming the same zero angle value, should be down by a factor of four over their measured value. If one accepts the reduction in cross-section due to multiple scattering, the cross-section should be even lower. A similar extrapolation of the angular distribution obtained in this experiment gives a much smaller zero angle value for the cross-section. This is again not surprising, since multiple scattering is expected to smooth out the strong peaking of the angular distribution at forward angles. (cf. Fig 3. page 14)

It is interesting in this connection to recall the double  $\gamma$ -ray work of Goldwasser, Koester and Mills<sup>37)</sup>. As described in the introductory chapter, these workers compared the  $\gamma$ -ray coincidence counting rates from hydrogen and helium at a laboratory angle of  $80^\circ$  for the  $\pi^0$ , and obtained roughly equal efficiency per nucleon for the photoproduction of  $\pi^0$ 's from hydrogen and helium up to a photon energy of about 200 MeV.

This comparison, though not strictly valid, as has been discussed earlier, at least gives us an idea for the order of magnitude of the cross-section.

At  $E_\gamma = 200$  MeV, this gives  $\left(\frac{d\sigma}{d\Omega}\right)_{\text{He}} \simeq 20 \mu\text{bn/sterad.}$

at a centre-of-mass angle of  $\sim 90^\circ$ . This agrees quite well with Stoodley's calculation with multiple scattering correction, Fig. XXVIII. Yamaguchi's<sup>59)</sup> calculation with pure impulse approximation gives a value which is about twice as high, and again agrees with Stoodley's corresponding curve. De Saussure and Osborne's result, however, is larger by a factor of four over that of Goldwasser et.al. The results of a single  $\gamma$ -ray work of Goldwasser and Koester<sup>38)</sup> also seem to point to the same conclusion (page 21). Thus the M.I.T. results seem to be consistently higher.

So far as the  $\text{He}^3$  cross-sections are concerned it is difficult to come to any definite conclusion, since the mechanism of their production is unknown. Cross-sections have been calculated on the assumption that they arise purely from the two-body photodisintegration process  $\gamma + \text{He}^4 \rightarrow \text{He}^3 + n$ . The initiating photon energies, however, were not quite the same at different angles, since the chamber pressure at each angle was adjusted to suit the kinematics of the  $\pi^0$  production process, and therefore, the results cannot be represented

as a proper angular distribution, more so since the excitation function is expected to be fairly steep in the energy range investigated. Even then, the roughly constant value of  $\sim 10 \mu\text{bn/sterad}$  at all angles from  $20^\circ$  to  $90^\circ$  is not in agreement with the  $\text{Sin}^2 \theta$  distribution obtained by De Saussure and Osborne. Probably at photon energies as high as 140 MeV, absorption of radiations other than electric dipole can be expected to be important. The value of the differential cross-section at  $90^\circ$ , viz  $9.6 \pm 2 \mu\text{bn/sterad}$ , at  $90 < E_\gamma < 138$  MeV is in good agreement with De Saussure and Osborne's result (Fig. III of their paper). The total cross-section assuming an isotropic angular distribution of average value  $10 \mu\text{bn/steradian}$  is  $10^{-27} \text{ cm}^2$  at a mean  $E_\gamma \sim 100$  MeV, which is down by a factor  $\sim 2$ , over De Saussure and Osborne's value (Fig. IV of their paper). A preliminary report of the work of Livesay <sup>60)</sup> of British Columbia, however, suggests that the cross-section for the process  $\gamma + \text{He}^4 \rightarrow \text{He}^3 + n$  falls off more rapidly than indicated by De Saussure and Osborne at higher energies. Livesay's value for the total cross-section is  $0.45 \pm .05 \text{ mb}$  at 40 MeV, but  $.1 \text{ mb}$  at 60 MeV. No definite conclusions can be drawn.

CONCLUSION.

The elastic photoproduction of neutral mesons from helium has been measured over an incident photon energy range from 220 - 320 MeV, and at centre-of-mass angles of  $70^\circ$ ,  $90^\circ$ ,  $115^\circ$  and  $135^\circ$  for the meson. The reaction has been identified by picking up the recoiling  $\alpha$ -particle at a given laboratory angle from a background of  $\text{He}^3$ 's produced by various competing photodisintegration processes. The investigation is thus more definite, and reliable than any conducted in the field so far. (Possible contribution from  $n$ - $\alpha$  and  $\gamma$ - $\alpha$  scattering processes were both estimated to be negligible).

The results show, that there is nothing drastically wrong with the impulse approximation as applied to photoproduction from a tightly bound nucleus. The agreement with theory, is however, only qualitative. The general trend in the modification of the cross-section due to multiple scattering correction seems to be borne out by experiment. Any quantitative comparison with theory, will however, have to await more refined calculations, which are increasingly difficult for a 4-body structure like the  $\alpha$ -particle.

As was pointed out on page 17 , Chapter I, there are three points of interest behind this experiment, viz -

- (1) Validity of the Impulse Approximation
- (2) Correction due to multiple scattering
- (3) Choice of a wave function for the Helium nucleus.

None of these points can, however, be considered to be definitely settled from the experimental results at the present stage of the theory, because of the large uncertainties in the calculations and the strong interdependence of the various factors involved. The main significance, and importance of an experiment like this, is therefore, to provide food for the theorist, and to stimulate him into more and more refined calculations.

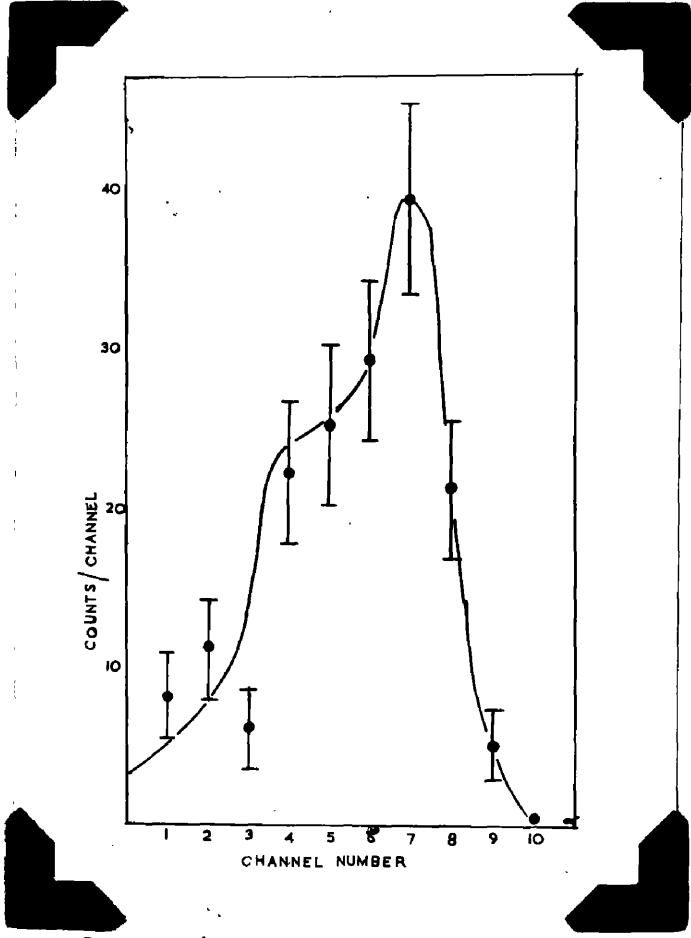


Fig.XXXI. He<sup>3</sup> & He<sup>4</sup> yields from the high energy photo-disintegration of O<sup>16</sup>, at 90° in the laboratory.

Appendix. He<sup>3</sup> and He<sup>4</sup> Yields from The High Energy Photodisintegration of Oxygen<sup>16</sup>.

The target pipe was filled with Oxygen gas to a pressure of  $1\frac{1}{2}$  atmosphere, and the recoiling helium nuclei at a laboratory angle of  $90^\circ$  were examined with the detector. The chamber pressure and all other conditions were exactly the same as in the corresponding run with helium. Fig. XXXI shows the histogram. It is seen that comparable numbers of He<sup>3</sup> and He<sup>4</sup> particles were produced. The yields/Oxygen nucleus, were roughly

$$9 \pm 1.5 \times 10^{-31} \text{ cm}^2/\text{sterad/MeV/Q for He}^3\text{'s}$$

$$12 \pm 2 \times 10^{-31} \text{ cm}^2/\text{sterad/MeV/Q for He}^4\text{'s}$$

and the energies of the nuclei varied roughly between 15 and 22 MeV at creation.

The yield of He<sup>3</sup>'s in appreciable numbers is rather interesting, in so far as it tempts one to look upon the O<sup>16</sup> nucleus as a cluster of 4  $\alpha$ -particles. Assuming that the  $\gamma$ -ray interacts with essentially one such sub-unit within the nucleus, and the rest of the nucleus sits as a spectator, the observed He<sup>3</sup>'s can be interpreted to arise essentially from the two-body photodisintegration process



and one can calculate the cross-section for the process for a quasi- $\alpha$ -particle within the  $O^{16}$  nucleus. Similar experiments<sup>61)</sup> on the quasi-deuteron model have been done. The observed yield of  $He^3$ 's from this reaction gives a value  $\sim 5 \mu\text{bn/steradian}$  at a mean  $E_\gamma \sim 127 \text{ MeV}$ , which is of the same order of magnitude as that for a free  $\alpha$ -particle. The argument, however, is highly crude and qualitative. It is difficult to justify the assumption that the rest of the nucleus does not take any part in sharing the momentum during the interaction between the  $\gamma$ -ray and the  $\alpha$ -particle, even if the latter did exist as a sub-unit. Thus the reaction kinematics is rather uncertain. Therefore, the number of  $\gamma$ 's responsible for the observed yield cannot be calculated with accuracy, nor the cross-section. Nevertheless, the result is of interest, and is compatible with the so called  $\alpha$ -particle model for which there is some evidence from other sources<sup>62)</sup>.

## REFERENCES.

- 1) Steinberger, J., Panofsky, W.K.H., and Steller, J.,  
Phys. Rev. 78, 802, 1950.
- 2) Panofsky, W.K.H., Steinberger, J., and Steller, J.,  
Phys. Rev. 86, 180, 1952.
- 3) Steinberger, J., and Bishop, A.S., Phys. Rev.  
78, 494, 1950.
- 4) Bishop, A.S., Cook, L., and Steinberger, J.,  
Phys. Rev. 80, 291, 1950.
- 5) Steinberger, J., and Bishop, A.S., Phys. Rev.  
86, 171, 1952.
- 6) Walker, R.L., Teasedale, J.G., Peterson, V.Z.,  
and Vette, J.I., Phys. Rev. 99, 210, 1955.
- 7) Tollestrup, A.V., Keck, J.C., and Worlock, R.M.,  
Phys. Rev. 99, 220, 1955.
- 8) Jenkins, T.L., Luckey, D., Palfrey, T.R., and  
Wilson, R.R., Phys. Rev. 95, 179, 1954.
- 9) Silverman, A., and Stearns, M., Phys. Rev.  
88, 1225, 1952.
- 10) Walker, R.L., Oakley, D.C., and Tollestrup, A.V.,  
Phys. Rev. 89, 1301, 1953.
- 11) Walker, R.L., Oakley, D.C., and Tollestrup, A.V.,  
Phys. Rev. 97, 1279, 1955.
- 12) Goldschmidt-Clermont, Y., Osborne, L.S., and  
Scott, M.B., Phys. Rev. 89, 329, 1953.
- 13) Goldschmidt-Clermont, Y., Osborne, L.S., and  
Scott, M.B., Phys. Rev. 97, 188, 1955.
- 14) Oakley, D.C., and Walker, R.L., Phys. Rev.  
97, 1283, 1955.
- 15) Koester, Jr., L.J., Phys. Rev. 98, 211, 1955.
- 16) Corson, D.R., MacDonald, W.S., and Peterson, V.Z.,  
Phys. Rev. 107, 577, 1957.

- 17) Cocconi, G., and Silverman, A., Phys. Rev. 88, 1230, 1952.
- 18) Mills, F.E., and Koester, Jr., L.J., Phys. Rev. 98, 210, 1955.
- 19) Koester, L.J., and Mills, F.E., Phys. Rev. 105, 1900, 1957.
- 20) Brueckner, K.A., and Watson, K.M., Phys. Rev. 86, 923, 1952.
- 21) Feld, B.T., Phys. Rev. 89, 330, 1953.
- 22) Sands, M., Teasdale, J.G., and Walker, R.L., Phys. Rev. 95, 592, 1954.
- 23) Cocconi, G., and Silverman, A., Phys. Rev. 88, 1230, 1952.
- 24) Bingham, H.H., Keck, J.C., and Tollestrup, A.V., Phys. Rev. 103, 1549, 1956.
- 25) Chew, G.F., and Lewis, H.W., Phys. Rev. 84, 779, 1951.
- 26) Wolfe, B., De Wire, J.W., and Silverman, A., Phys. Rev. 99, 268, 1955.
- 27) Rosengren, J.W., and Baron, N., Phys. Rev. 101, 410, 1956.
- 28) Davis, H.L., and Corson, D.R., Phys. Rev. 99, 273, 1955.
- 29) Belousov, A., Tamm, E., and Kucenko, A., Nuovo Cimento Supplement, Series X, Vol. III, p.32, 1956.
- 30) Wilson, R.R., Phys. Rev. 86, 261, 1952.
- 31) Aschenbrenner, F.A., Phys. Rev. 98, 657, 1955.
- 32) Stokes, R.H., Northrop, J.A., and Boyer, K., Rev. Sci. Inst., 29, 61, 1958.
- 33) Chappellear, J., Phys. Rev. 99, 254, 1955.
- 34) Chew, G.F., and Wick, G.C., Phys. Rev. 85, 636, 1952.
- 35) Butler, S.T., Phys. Rev. 87, 1117, 1952.

- 36) Laing, E.W., and Moorhouse, R.G., Proc. Phys. Soc. 70, 629, 1957.
- 37) Goldwasser, E.L., Koester, Jr., L.J., and Mills, F.E., Phys. Rev. 95, 1692, 1954.
- 38) Goldwasser, E.L., and Koester, Jr., L.J., Nuovo Cimento Supplement 4, 950, 1956.
- 39) De Saussure, G., and Osborne, L.S., Phys. Rev. 99, 843, 1955.
- 40) Birks, J.B., Phys. Rev. 84, 364, 1951.
- 41) Jeans, J., "The Mathematical Theory of Electricity and Magnetism", p. 275, Cambridge University Press.
- 42) Bunemann, O, N.R.C. Report, P.D. 285, 1946.
- 43) Wilkinson, D.H., "Ionization Chambers and Counters", page 77, Cambridge University Press.
- 44) Landau, L., J. Phys. U.S.S.R., 8, 201, 1944.
- 45) Symon, K.R., Thesis, Harvard University, 1948, unpublished.
- 46) Rossi, B., "High Energy Particles", p. 31, Prentice Hall Incorporated.
- 47) Harvey, B.G., Jackson, H.G., Eastwood, T.A., and Hanna, G.C., Canadian Journal of Physics, 35, 258, 1957.
- 48) Rich, M., and Madey, R., Range Energy Tables, U.C.R.L. 239, 1954.
- 49) Bates, Proc. Roy. Soc. A, (1924) 106, 622.
- 50) Aron, W.A., Hoffman, B.G., and Williams, F.C., Range Energy Curves, p.74, AE CU - 663, 1951.
- 51) Corson, D.R., De Wire, J.W., McDaniel, B.D., and Wilson, R.R., "The Cornell 300 MeV Synchrotron" pp.62.
- 52) Heitler, W., "The Quantum Theory of Radiation", p.170, second edition, Oxford University Press.

- 53) Blaton, Danske Videnskabernes Selskab, 24  
(1946-50), Paper No. 20.
- 54) Chew, G.F., Phys. Rev. 95, 1669, 1954.
- 55) Irving, J. Proc. Phys. Soc. 66, 17, 1953.
- 56) Hofstadter, R., McAllister, R., and Wiener, E.,  
Phys. Rev. 96, 854, 1954.
- 57) Cladis, J.R., Hess, W.N., and Moyer, B.T.,  
Phys. Rev. 87, 425, 1952.
- 58) Irving, J., Phil. Mag. 42, 338, 1951.
- 59) Yamaguchi, Y., Progress of Theoretical Physics,  
13, 459, 1955.
- 60) Livesay, D.L., Preliminary report from the  
Proceedings of the Photonuclear Conference  
April 30 - May 1, 1958, National Bureau of  
Standards, Washington, D.C.
- 61) Wattenberg, A., Odian, A.C., Stein, P.C., Wilson, H.,  
and Weinstein, R., Phys. Rev. 104, 1710, 1956.
- 62) Moszkowski, S.A., Handbuch der Physik, 39, 460, 1957.
- 63) Boicourt, G.P., and Brolley, J.E., Rev. Sci. Instr.  
25, 95, 1954.